8-2018

A device for autonomous accurate measurement of sediment mass in a water sample

Hayden Nicholas Jordan
University of Tennessee, hjordan3@vols.utk.edu

To the Graduate Council:

I am submitting herewith a thesis written by Hayden Nicholas Jordan entitled "A device for autonomous accurate measurement of sediment mass in a water sample." I have examined the final electronic copy of this thesis for form and content and recommend that it be accepted in partial fulfillment of the requirements for the degree of Master of Science, with a major in Biosystems Engineering.

John B. Wilkerson, Daniel C. Yoder, Major Professor

We have read this thesis and recommend its acceptance:

John R. Buchanan, John S. Tyner

Accepted for the Council:
Dixie L. Thompson

Vice Provost and Dean of the Graduate School

(Original signatures are on file with official student records.)

A device for autonomous accurate measurement of sediment mass in a water sample

A Thesis Presented for the
Master of Science
Degree
The University of Tennessee, Knoxville

Hayden Nicholas Jordan
August 2018

ACKNOWLEDGEMENTS

I would like to thank my major advisors, Dr. John Wilkerson and Dr. Daniel Yoder, for providing the funding for this research as well as the numerous hours of guidance. I would also like to thank my committee members, Dr. John Buchanan and Dr. John Tyner, for giving me the support needed to engineer a successful design.

Mr. David Smith of the Biosystems Engineering and Soil Science (BESS) Department aided in the design and cutting of the printed circuit boards. Mr. Scott Tucker of BESS helped machine several of the components used on the system.

I would like to thank Jonathan Yoder for his consultation throughout the design process as well as his help with the code design. I would also like to thank Jordan Brewer for his assistance in conducting laboratory tests and his creation of the three-dimensional drawings used in the paper.

Finally, I must express my profound gratitude to my family as well as my friends as they provided continuous encouragement and support throughout my years of study.

ABSTRACT

Sediment is a major water pollutant causing damage to aquatic ecosystems, clogging waterways, and filling reservoirs. Regulatory agencies like EPA and TDEC want to regulate sediment release from disturbed land uses (e.g., construction, mining, or forestry) by limiting measured discharge, as they do for contaminants from factories or wastewater treatment plants. However, they rather typically settle instead for simply requiring application of pre-approved BMPs applied to the site in a specified manner, because measuring sediment discharge is such a difficult, expensive, labor-intensive, and time-consuming process. In order to require measured sediment discharge, there must be a system that can accurately and easily measure the sediment concentration in a water sample in-situ and in near real time.

This project developed a measurement system to accurately quantify a sample's sediment mass under either gravity-fed or pumped inflow conditions. The system analyzes a 0.5 L sample every 90 s and measures the sample's sediment mass to within 0.25 g or 5% of the known added mass (whichever is larger) across the range from 1,200 – 120,000 mg L^{-1} of sample. Additionally, the data acquisition system stores data in non-volatile memory and supports wireless data transfer while minimizing power consumption.

Preliminary testing shows that with human interaction the system can meet the sediment measurement accuracy requirements for sand, silt loam, and clay loam. However, errors introduced by four different elements of current system dynamics prevent the automation of the data analysis and thus total system success. Once optimized through several additional redesigns, the system could provide a significantly-improved method of regulating discharge from construction sites, as well as providing support for general stream or river water quality work.
.

TABLE OF CONTENTS

LIST OF TABLES

LIST OF FIGURES

CHAPTER ONE
INTRODUCTION

Background

One of the major contributors to the pollution of worldwide waterways is sediment, which is delivered to streams and rivers via runoff from storm events. Disturbed lands with little cover are more prone to sediment delivery during a rainfall event (USEPA, 2009), so mining, logging, agriculture, and construction are a few of the major land practices that contribute to sediment delivery. When no measures are put into place to remove sediment from runoff, it is transported offsite and discharged into downstream waterways. Increased sediment delivery can alter stream ecosystems via the clogging of streambed substrates, reduction of macro-invertebrate habitats, and the changing of downstream channel morphology (Ehrhart et al., 2002). Also, sediment decreases the storage capacity of reservoirs and degrades the quality of water for municipal, industrial, and recreational uses.

Following the passing of the Clean Water Act, discharging pollutants from point sources into United States waters requires a National Pollutant Discharge Elimination System (NPDES) permit. State and federal regulatory agencies like the Environmental Protection Agency (EPA) oversee the issuing of these NPDES permits, with the construction industry receiving most of the permits for discharges from disturbed lands. After specifically identifying the construction industry as a point source category for which the EPA intended on imposing stricter effluent guidelines and performance standards, the EPA chose not to reform construction discharge regulations in 2004 (MacCurdy, 2010). The ensuing backlash from environmental groups resulted in a Ninth Circuit Court ruling mandating that the EPA develop effluent limitation guidelines and new source performance standards for the construction industry by 1 December, 2008, and that EPA declare a final rule by 1 December, 2009 (MacCurdy, 2010).

Because of the difficult and time-consuming process of extracting, filtering, and drying water samples to determine sediment mass, the EPA chose to not require actual sampling of stormwater discharges from construction sites, and instead proposed estimating sediment loads using turbidity as a surrogate (USEPA, 2009). Turbidity is a commonly measured water quality parameter, and measurements are easily captured *in-situ* and in real time using relatively inexpensive turbidity sensors. Turbidity is the cloudiness of a water sample and is determined based on the propensity of particles to scatter or block a light beam focused on them. The more light scattered or blocked by the sediment particles, the higher the recorded turbidity measurement. In 2008 the EPA proposed the requirement that large construction sites (more than 30 acres) meet an effluent turbidity limit of 13 nephelometric units (NTUs) (MacCurdy, 2014). After revising the proposed rule in 2009 to 280 NTUs for construction sites of 10 acres or more, the EPA further revised the rule in 2014 to no numeric turbidity effluent limits due to the proposed rule being deemed “infeasible”, defined as “not technologically possible or not economically practicable and achievable in light of best industry practices” (MacCurdy, 2014). Furthermore, the numeric turbidity method is complicated by the fact that turbidity measurements must be calibrated against more standard measures of sediment load to provide

true quantitative values. This is because many site-specific factors affect turbidity readings, including especially soil characteristics, but also water chemistry, sources of tannins, etc. For example, a small amount of clay can result in a high turbidity reading due to its ability to stay suspended within a water column, while the same mass of sand particles will settle out quickly, potentially causing less light to be scattered. Additionally, it is possible for a single sand particle to block much of the light beam from the turbidity sensor for a short time, which may or may not result in a high turbidity reading depending on how the sensor is being read. These biases in turbidity measurements may result in poor estimates of sediment leaving a construction site without specific on-site calibration, making it difficult to utilize turbidity as a reliable means of determining sediment load.

Alternative Methods

In order to characterize the current situation or to demonstrate sediment removal by various practices (*e.g.,* sediment basins, permanent stormwater practices, etc.), one needs to be able to easily measure the sediment concentration. The American Society for Testing and Materials (ASTM) Standard Test Method D 3977-97 lists three methods to determine suspended-sediment concentration values in water (ASTM, 2013). Test Method A applies to sediments that settle under the influence of gravity and with samples ranging from 0.2 to 20 L in volume and 5 to 550,000 mg L^{-1} of sediment concentration. It determines suspended-sediment concentrations by allowing time for settling then siphoning away the supernatant water in the sample, and sampling and drying a portion of that supernatant such that a dissolved-solids correction factor can be applied. Finally, drying and weighing the settled sediment allows for calculation of the suspended-sediment concentration.

Test Method B applies to samples containing sand concentrations less than 10,000 mg L^{-1} and clay concentrations less than 200 mg L^{-1}. Sediment need not be settleable in this method because filters are used to separate water from the sediment, and correction factors for dissolved solids are not required. First, a glassfiber disk filter is used to separate a weighed sample. Drying and weighing the disk and captured sediment allows for calculation of the sediment concentration.

Test Method C is applicable if two concentration values are required: one for sand-size particles and one for the combination of silt and clay-size particles. The silt-clay fraction need not be settleable for this method. The sample is poured through a sieve with 62 or 63 μm openings, and the material caught by the sieve is dried and weighed. A small, measured aliquot of the water and sediment passing through the sieve is then weighed and dried to determine the total fine sediment mass. Sieving and aliquot extraction can be performed either at the sampling site or in the laboratory.

These three standard methods are the standard ways of measuring sample sediment mass, but the methodology is slow, laborious, and therefore expensive. None of the methods are easily adaptable to *in-situ* automated measurement.

Alternative suspended sediment measurement techniques make use of various forms of instrumentation. Acoustic methods use high frequency sound waves emitted from a transducer (Walling and Horowitz, 2005). The strength of the back-scatter as it hits the sediment determines the size and the concentration of the sediment particles. This approach has the disadvantage of

the acoustic signal being attenuated by a high particle concentration within the volume. Another similar approach uses focused beam reflectance, which measures the time of reflection of a laser beam as it encounters particles within a volume, determining the size and concentration of sediment (Walling and Horowitz, 2005). However, this method tends to be expensive and provides only point measurements rather than measurements over time.

A study conducted by Lewis and Rasmussen (1996) proposes using a pressure transducer to accurately measure sediment concentrations in water based on the increase in relative fluid density caused by the sediment. The study attributes the change in pressure at the bottom of a water column containing sediment to the change in specific weight caused by the addition of sediment particles to the water. The results of the study confirm that pressure can be used to measure sediment concentrations in water, but the study was only conducted on a laboratory scale using glass beads as a replacement for sediment particles, and was never examined as a robust field measurement system. Furthermore, a study conducted by Durner et al. (2017) proposes a method that determines the particle-size distribution (PSD) of a water sample based on the pressure in the suspension at a selected depth. Knowing the PSD allows one to better understand the physical and chemical properties of the suspended soil. This new analysis method measures PSD at very high resolutions, but it is limited by the depth under the water surface that the pressure transducer is placed. Additionally, this method recommends that sand be removed first by sieving such that relative particle size is evenly distributed.

Design Need

The current situation thus leaves a need for a system that can accurately and easily measure the sediment concentration in a water sample *in-situ*, autonomously (without human interaction), and in close to real time. Such a system could be used for situations like the construction-site dilemma facing EPA, general stream or river water quality work, or for measuring sediment movement from test areas. A system with these capabilities provides the means to regulate sites using a measurement-based standard similar to that used for most NPDES permits, getting away from the implementation-based approach currently being used. Therefore, the goal of this project is to answer the question arising from EPA's ill-fated attempt to provide an easily-measured surrogate for sediment load: Can a device be designed such that it allows for an autonomous, simple, direct, and accurate measurement of sediment load?

CHAPTER TWO
DESIGN APPROACH

Design Objectives

The overall project goal is to develop a measurement system that can autonomously yet accurately quantify the sediment concentration of a sample taken from any source. To accomplish this goal, the design should be able to capture a precise, known volume of water and sediment mixture from a pumped or gravity-fed inflow such that it can autonomously (with no human interaction) analyze each sample to obtain its sediment mass with high accuracy across the sediment concentration range of 1,200 mg L^{-1} to 120,000 mg L^{-1} of sample (roughly 0.6 g to 60 g for a 0.5 L sample). Additionally, the design must store the data as non-volatile memory such that it can be transmitted wirelessly. Finally, the system needs to be designed such that it can operate autonomously in a demanding outdoor environment.

Conceptual System Design

The sediment analysis device designed by this project is one element in a total system needed to determine the sediment mass contribution from a source such as a sediment basin discharge. The total system requires the elements shown below in Figure 2.1, including the following: 1) time-varying flow rate measurement, enabling determination of flow volume associated with each sampled concentration; 2) a method of extracting a representative sample from that flow; and 3) the sediment analysis device proposed by this study. This final element was chosen as the first for further development and study because the other elements have acceptable methods, though each can certainly be improved.

The sediment concentration device accommodates flow from a gravity-fed or pumped source. This enables implementation in various scenarios, such as water flowing from a sediment basin or pumped from a stream. As described previously, the measurement technique for the sediment analysis device is based on the Lewis and Rasmussen (1996) approach of measuring pressure at the bottom of a water filled column. In general terms, the system makes use of the density difference between clean water (normally very near 1.0 g cm^{-3}) and sediment (normally about 2.65 g cm^{-3}). The pressure differential between the collected sample and a reference column of the same height containing pure water (column "Reference" in Figure 2.2) indicates the sediment mass.

Because the heights of the two columns are equal, any difference in the pressure between the two columns must correspond to the difference in density, which will be dependent on the amount of sediment suspended in the sample column and its specific gravity.
The pressure in each column is defined by the following equation:

$$P = \rho g h$$

where
P = pressure (Pa)
ρ = fluid density (g m^{-3})

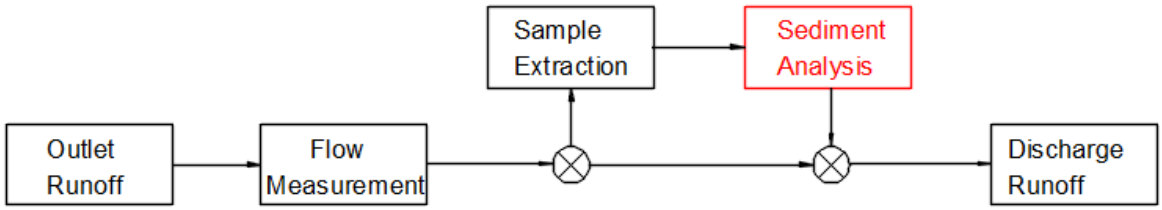

Figure 2.1. A flow diagram of how a sediment-laden flow passes through the three components of a complete sediment mass measurement system. As shown in red, the sediment analysis component is the focus of this proposal.

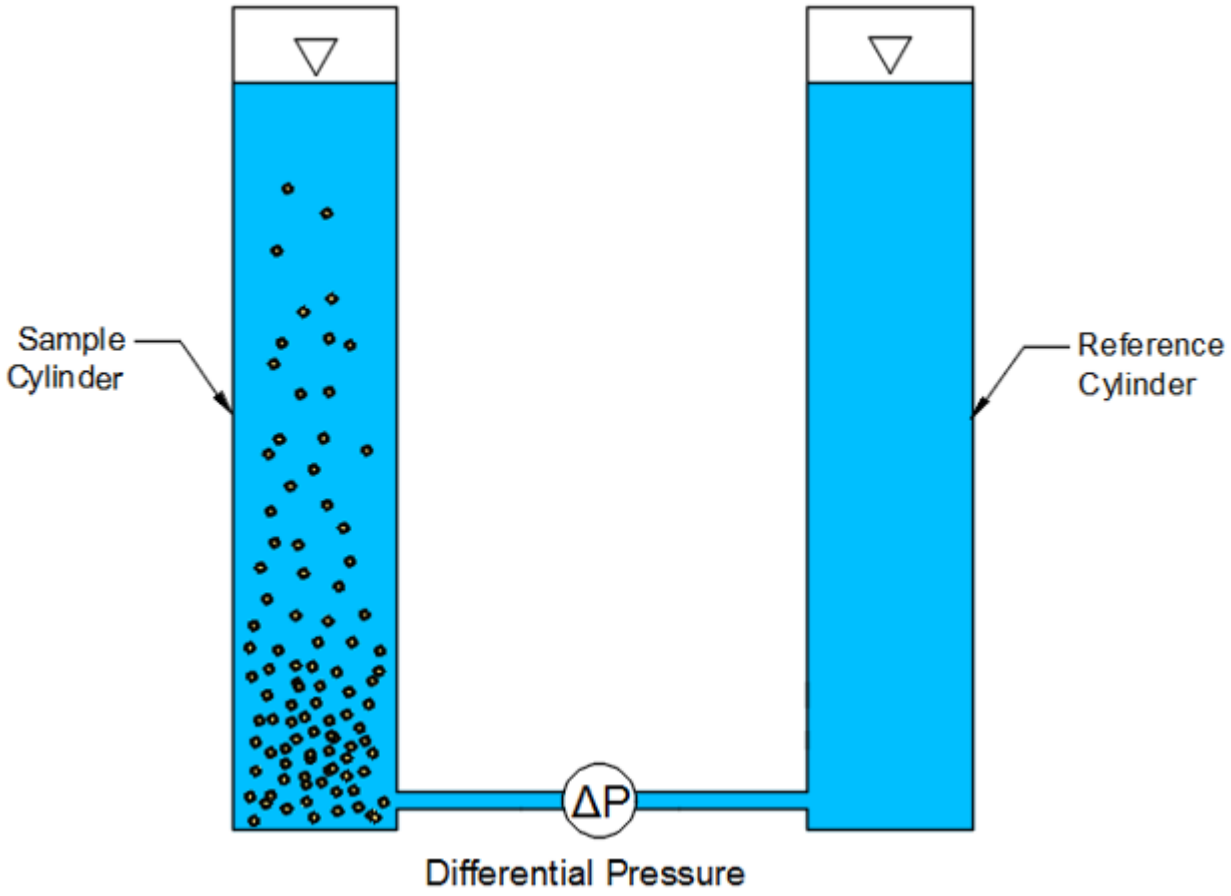

Figure 2.2. Sediment mass is calculated based on the differential pressure between a sample column and a reference column containing distilled water.

g = gravitational constant (m s^{-2})
h = height(m).

Since the columns have the same h and g, any pressure differences must be caused by differences in ρ, which will be caused by the sediment mass in the sample column.

As a sediment particle settles through the water it quickly reaches terminal velocity, at which point the downward force due to gravity equals the upward drag force of the water on the sediment. Since the water exerts an upward force on the sediment, the settling sediment exerts an equal and opposite downward force on the water. That force is equal to the excess weight of the sediment relative to the water it is displacing, measured at the bottom of the column as a resulting change in the overall pressure. However, once the sediment settles and rests on the bottom of the column, its excess weight is borne by the column itself rather than the water, so it will not be reflected in the water pressure. A relatively crude pressure transducer on a hand-manipulated column proved this concept (Lewis and Rasmussen, 1996). This testing, however, did not involve calibration nor use of precise volumes.

In addition to compensating for temperature and other minor impacts on water density, the reference column allows use of a differential pressure transducer with a full-scale reading representing only the maximum expected excess sediment weight in the sample column. If measuring the sample column pressure in its entirety as was done by Lewis and Rasmussen (1996), the additional pressure caused by the sediment excess weight will be a very small part of the total signal that also includes the weight of the water. Using the reference column essentially "counter-balances" the mass of water, allowing the full-scale pressure reading to reflect only the expected sediment excess weight.

The system's critical element is a 0.5 L test column (labeled "Sample" in Figure 2.3) with valves at both ends. The following analysis led to the selection of the 0.5 L volume. It is possible that large soil aggregates (~0.2 g) can become suspended in the sampled flow. The presence or absence of one of these aggregates could greatly affect measurements taken if the measured volume is too small. Therefore, a sample volume must be chosen such that one of the controlling elements (a soil aggregate) does not make a significant impact on the measurement (sediment concentration). For example, it is impractical to select 0.5 mL as the sample volume for the study's sediment concentration analysis, because the presence or absence of a single large soil aggregate would dominate the measured sample. In general, it is desired that the sample volume be large enough that the controlling element represents an impact in the same range as the desired accuracy. For this study, the sediment pumped to the sample column does not contain aggregates. Therefore, sand (with an approximate mass of 0.025 g per grain) is the controlling element. Because sand does not aggregate and its mass corresponds to 5% of the total mass the system must measure at the lowest concentration, a sample volume of 0.5 L is appropriate. For sampling a flow where very large stable aggregates are expected, the column could be scaled accordingly.

In operation, the valves at both ends of the sample column are normally open to allow the inlet flow to pass through the "Fill" valve into the cylinder and out through the open bottom "Drain" valve (Figure 2.3). At the start of a sampling cycle the Drain valve closes and the column fills (Figure 2.4). Once the sample column fills to overflowing as measured by the liquid level sensor, the inflow is diverted to a discharge system, and the Fill valve closes (Figure 2.5).

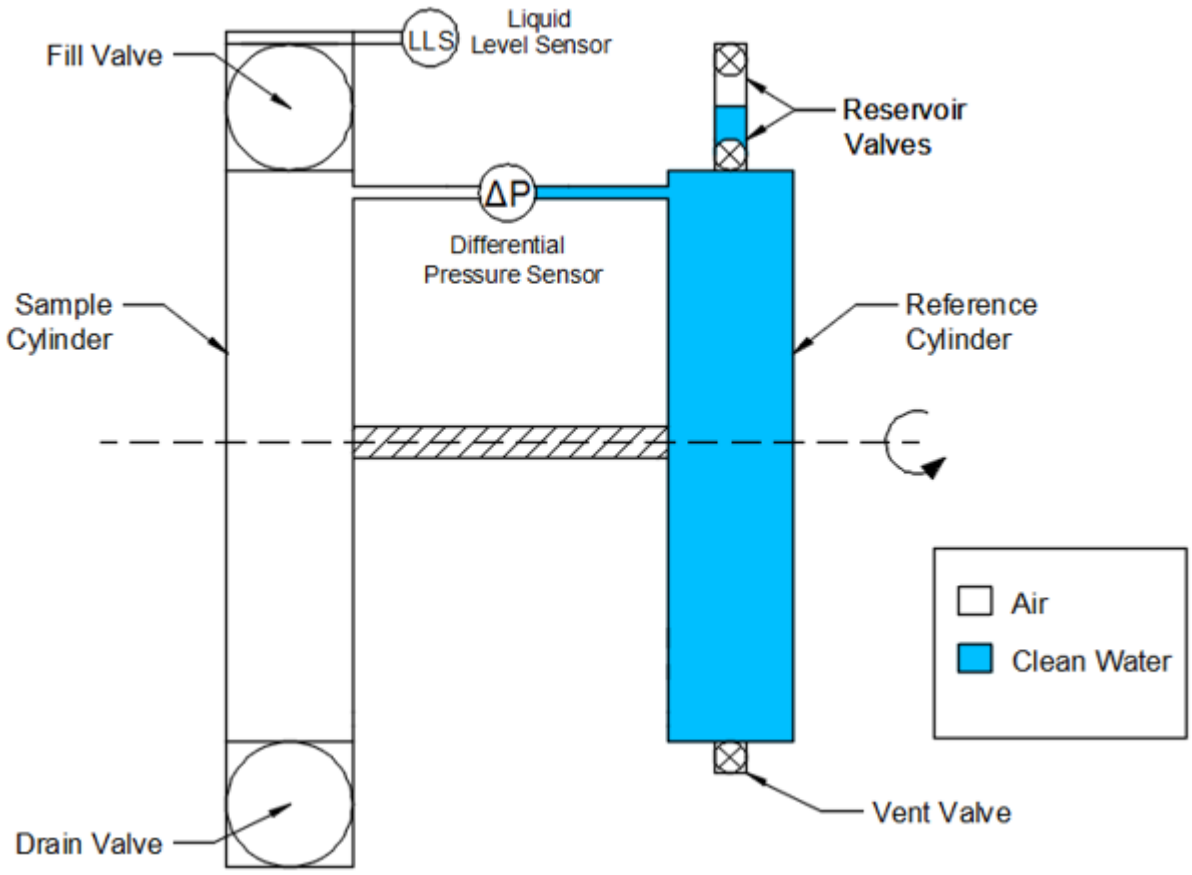

Figure 2.3. The general design for the sediment concentration analysis apparatus. The Sample column holds the 0.5 L sample captured from the inflow, while the Reference column holds 0.5 L of clean water.

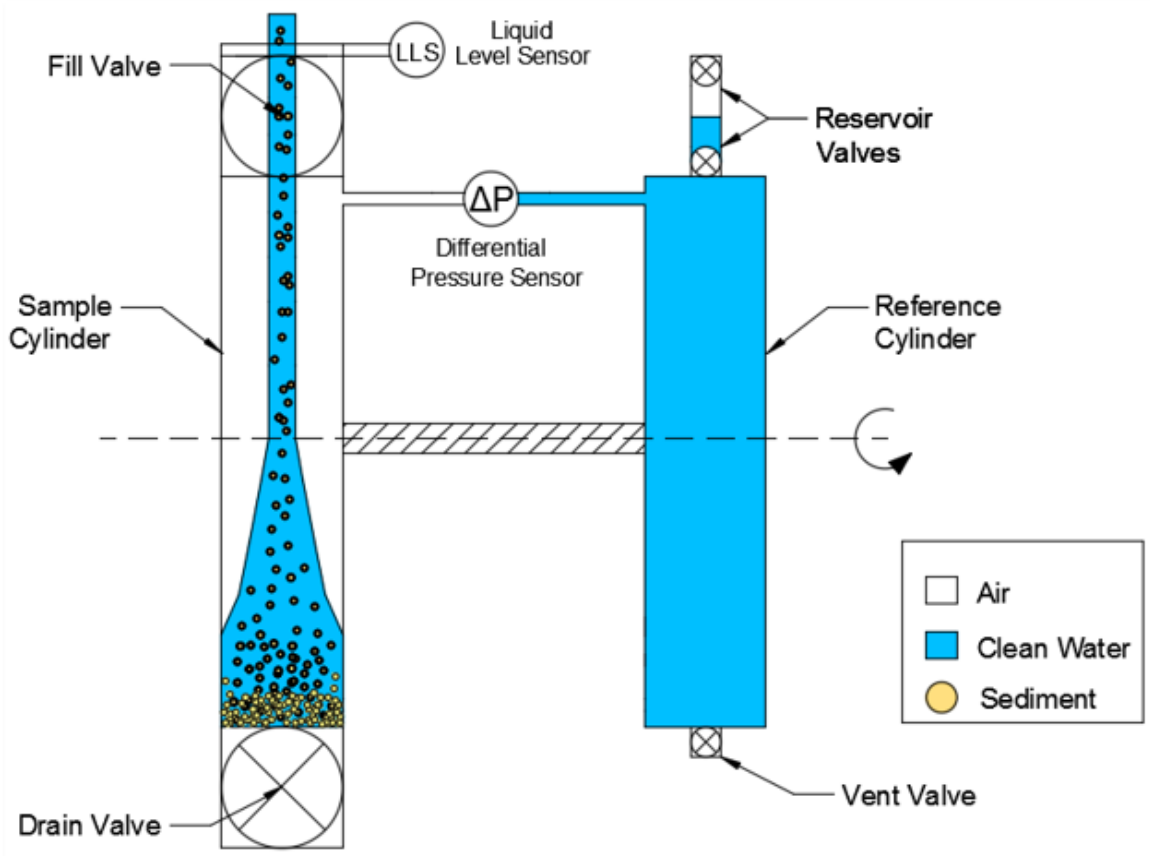

Figure 2.4. The general design for the sediment concentration analysis apparatus during filling. The Drain valve is closed, and the Sample cylinder fills with sediment-laden water.

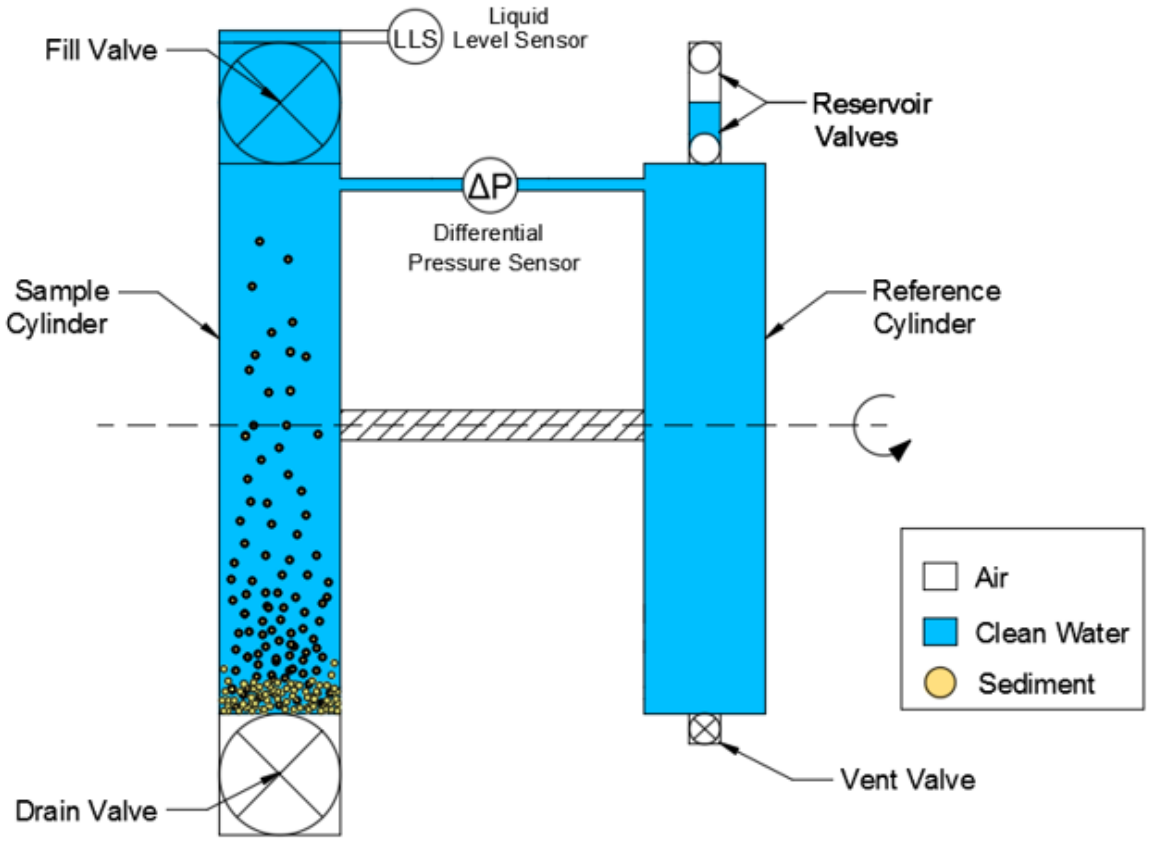

Figure 2.5. The general design for the sediment concentration analysis apparatus once the Sample column has filled as determined by the liquid level sensor. At this point, the Reservoir valves are opened to the atmosphere such that a constant height is maintained within the Reference column. As shown in the figure legend, the Sample column contains a combination of settled coarse and suspended fine sediment.

This procedure ensures that each time the system captures a precise, repeatable, known volume for analysis. Based on repeated lab testing described more fully below, this two-valve system captures a 0.5 L volume repeatable within 0.02%.

Once the sample column fills with sediment-laden water from the inflow, the two "Reservoir" valves at the top of the reference column open to the atmosphere as shown in Figure 2.5. An additional small reservoir of water contained between the two valves allows the surplus water to move into or out of the reference column if the cylinder volume changes slightly due to thermal expansion of the water and/or cylinder. Once those valves are closed again, the two columns should both be completely full with identical heights of water.

As the sample column fills with dirty water at the beginning of the cycle, the heavier sand and silt particles will have time to settle out of the water and rest on the bottom of the column. Very coarse sand (2.0 mm diameter) falls through water at standard conditions with a terminal velocity of about 3.43 m s^{-1} (11.2 ft s^{-1}). Using a cylinder with a length of 0.3 m, this very coarse sediment falls from top to the bottom in ninety milliseconds, meaning that it is possible for the larger sediment to settle at the bottom long before the sample cylinder is completely full of water. Since the excess weight of these particles is no longer borne by the water of the sample but rather by the bottom of the cylinder, a pressure reading taken by a sensor at the bottom of the sample column would not represent the entire sample sediment mass, but only that still suspended. The pressure reading will decrease as particles settle due to the decrease in the density, as shown in Figure 2.6. To compensate for the settling of sediment particles, once the sample cylinder is full (as determined by the liquid-level sensor) and all valves are closed, the entire apparatus is quickly inverted 180° by an electric motor, such that the settled sediment goes from being on the bottom of the cylinder to being at the top of the water column, as shown in Figure 2.7. This re-suspends the sediment particles and allows the differential pressure sensor (originally located at the top of the columns, but after inversion now at the bottom) to obtain an accurate differential pressure measurement corresponding to the total sediment mass in the water column before any sediment has a chance to settle to the new cylinder "bottom".

Note that this system allows not only for measurement of the total sediment mass (while it is in suspension and therefore is supported by the water), but perhaps also some measure of the sediment size distribution by recording how the pressure changes over time as the sediment settles to the bottom. It is thought that adding multiple pressure transducers at different depths in the sample column may also aid in capturing the sediment size distribution, but this requires further research not performed by this study.

After inverting the cylinders, the sample column Drain valve (now at the top due to inversion) and the reference column Vent valve are opened, as seen in Figure 2.7. This allows both cylinders to vent to atmospheric pressure, preventing either column from becoming pressurized by thermal changes causing expansion or contraction of the columns. After capturing the differential pressure reading, all valves close and the assembly rotates back to its original position. The Drain and Fill valves on the sample column open and the inflow is again passed through the column to flush the cylinder (Figure 2.8), setting the stage for a new sample cycle. Pressure readings from each sample cycle are written to non-volatile memory via a microprocessor, and the stored values are wirelessly transmitted.

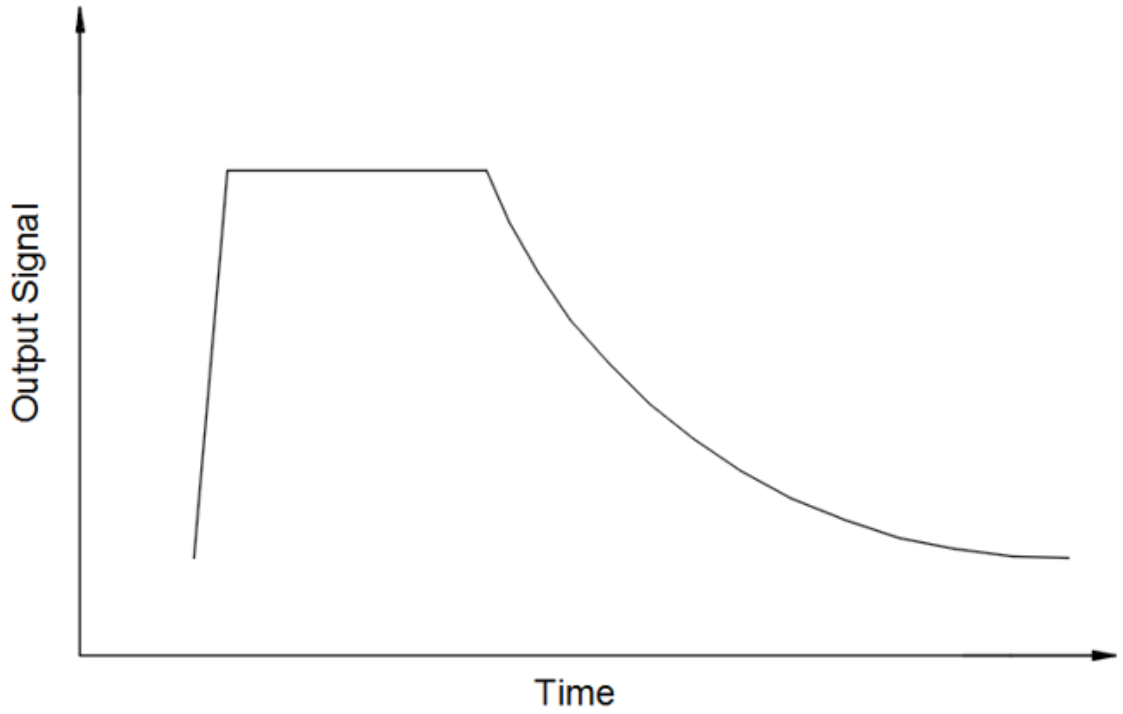

Figure 2.6. This figure depicts a theoretical pressure transducer signal as the sediment in the sample column goes from being suspended to settling at the bottom of the column. The initial increase in signal corresponds to all the sediment suspended within the sample column. As soon as the first sediment particle falls below the pressure transducer, the signal begins to decline similar to that of exponential decay.

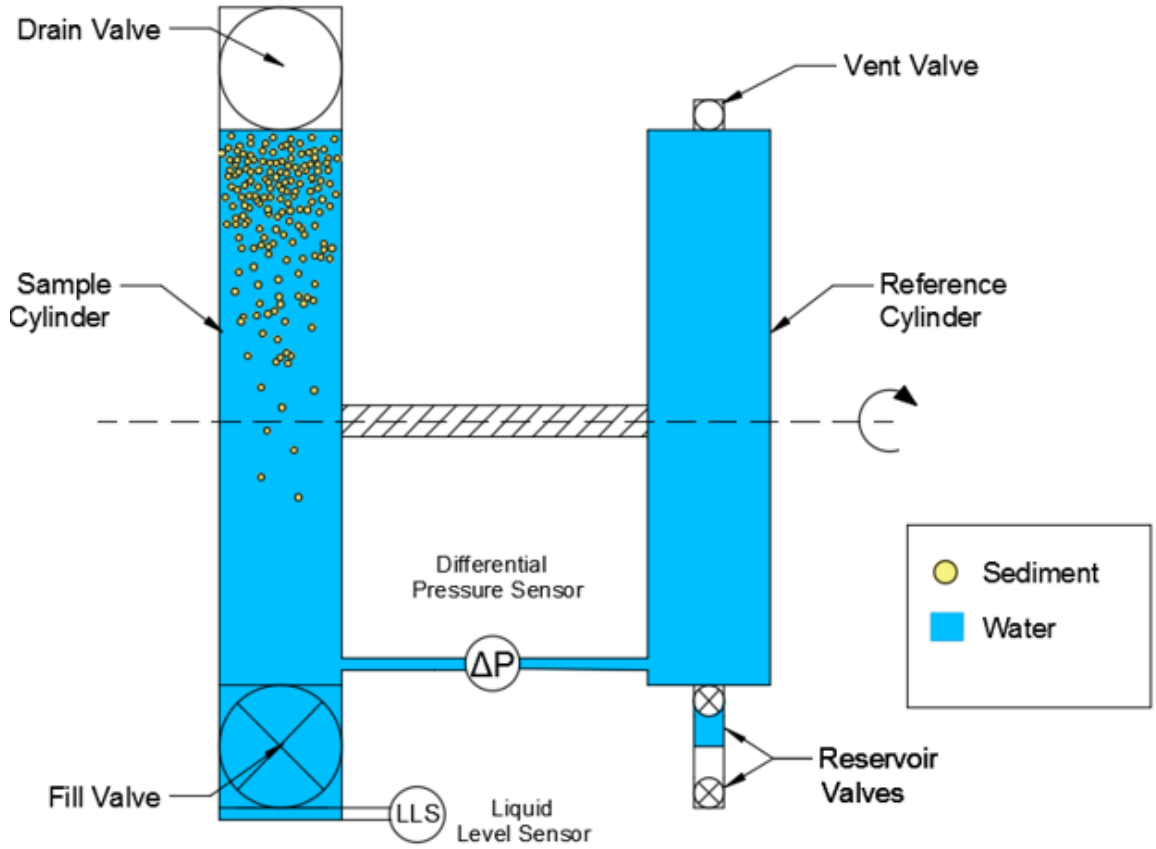

Figure 2.7. The general design for the sediment concentration analysis apparatus after inversion. Both the Drain valve and the Vent valve are open to the atmosphere to prevent column pressurization. A differential pressure sensor between the two cylinders captures the differential pressure during this period.

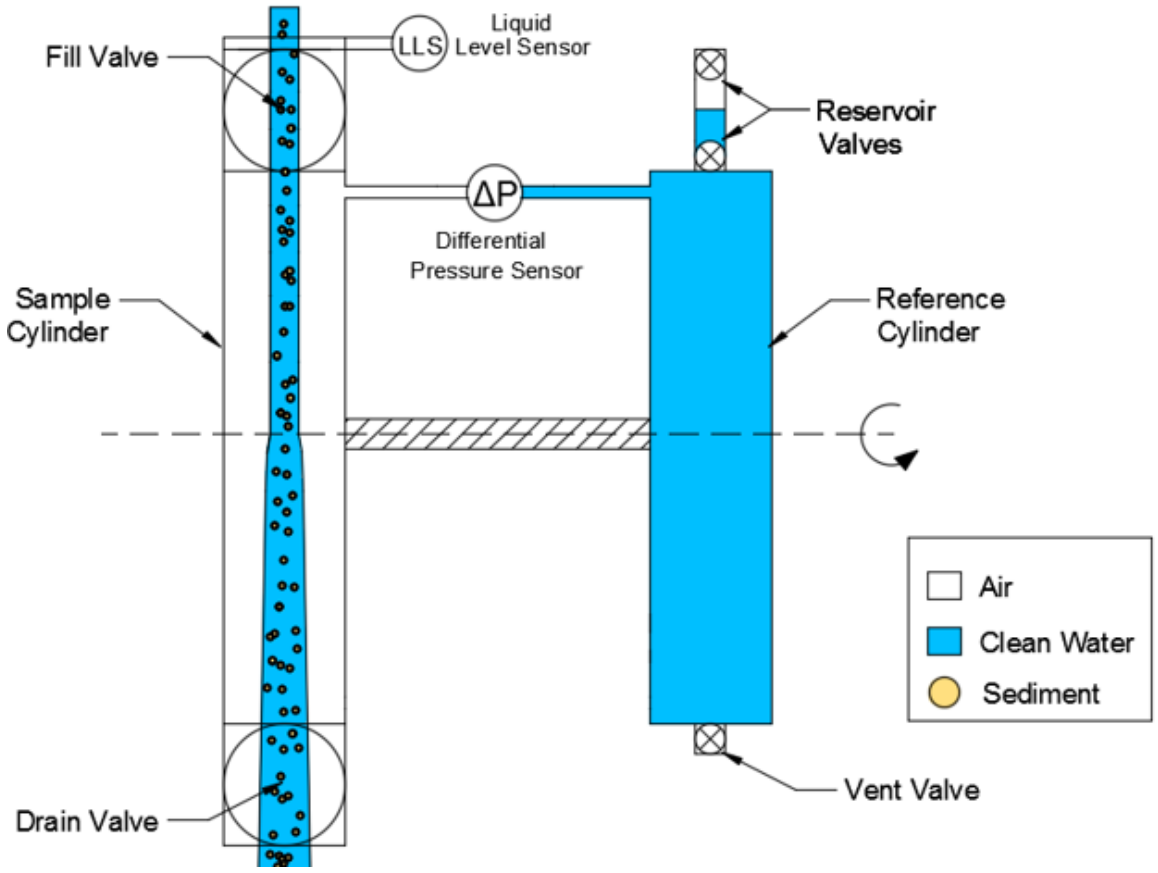

Figure 2.8. The general design for the sediment concentration analysis apparatus during flushing between samples. Both the Drain valve and the Fill valve are open, allowing the incoming flow to pass through the Sample column.

CHAPTER THREE
PROTOTYPE DESIGN

Components

The general system design of the system is based on its five major functions: 1) capture a precise sample volume; 2) capture a differential pressure reading reflecting the sample suspended sediment; 3) store the pressure reading for each sample; 4) operate autonomously; and 5) operate in an energy efficient manner. Addressing questions related to the system functions influenced the selection of the various components that make up the overall sediment analysis device shown in Figure 3.1. Unless otherwise specified, all references to component mounting are with respect to the system in the "Fill" position shown in Figure 2.8.

Column Assembly

The sediment analysis device must first perform the function of obtaining a precise volume. Repeatedly capturing a known sample volume is critical to the calculation of the amount of sediment concentration contained in the sample, and to allow comparison to the reference column with its known volume. To correlate the hydrostatic pressure measured at the bottom of the column to the addition of sediment mass in the sample, the volume of the sample must be constant. Keeping in mind that the system can operate under pipe-fed and gravity-fed inflows, the idea of using a valve on either end of a vertical cylinder arose as a solution for capturing the precise volume. This design not only allows for a simple method for sample capture, but also allows gravity and the force of the inflow to flush the column between samples. The sample cylinder should not contain areas that obstruct the flow of sediment-laden water that might accumulate sediment. Therefore, the selected container volume design implements two valves on either end of a PVC pipe. Not only does PVC have a smooth inner surface, but it is a cost-efficient material that can be easily mounted to ball valves. These ball valves have a clear opening essentially equal to the pipe diameter, allowing a water flow path with minimal obstruction. Initial proof of concept testing showed that two ball valves on either end of a length of PVC capture a repeatable sample volume.

Based on these results, the design uses two cylinders of 1" schedule 40 clear PVC cut at lengths of ~0.91 m (3 ft), used as the sample and reference cylinders. Clear PVC provides a means for visually observing the sediment as it falls through the sample cylinder. The 0.91 m length of the 0.5 L test volume provides an adequate sampling time (based on a particle's fall velocity) while also keeping a reasonable fill time (~ 5 s based on 5.7 L min^{-1} [1.5 gpm] inlet flow).

The design must operate autonomously, so initial research examined different types of electrically-powered valves. As mentioned, the valve openings on the sample cylinder need to be large enough that they do not obstruct the flow and can pass small soil aggregates. Given that the inside diameter of the schedule 40 Clear PVC is 2.66 cm (1.049 in), the Fill and Drain valves for the sample cylinder are two 1" 12V Deelat DC Motorized SS304 ball valves, allowing for negligible flow obstruction. Additionally, these valves draw 150 mA, which is small relative to

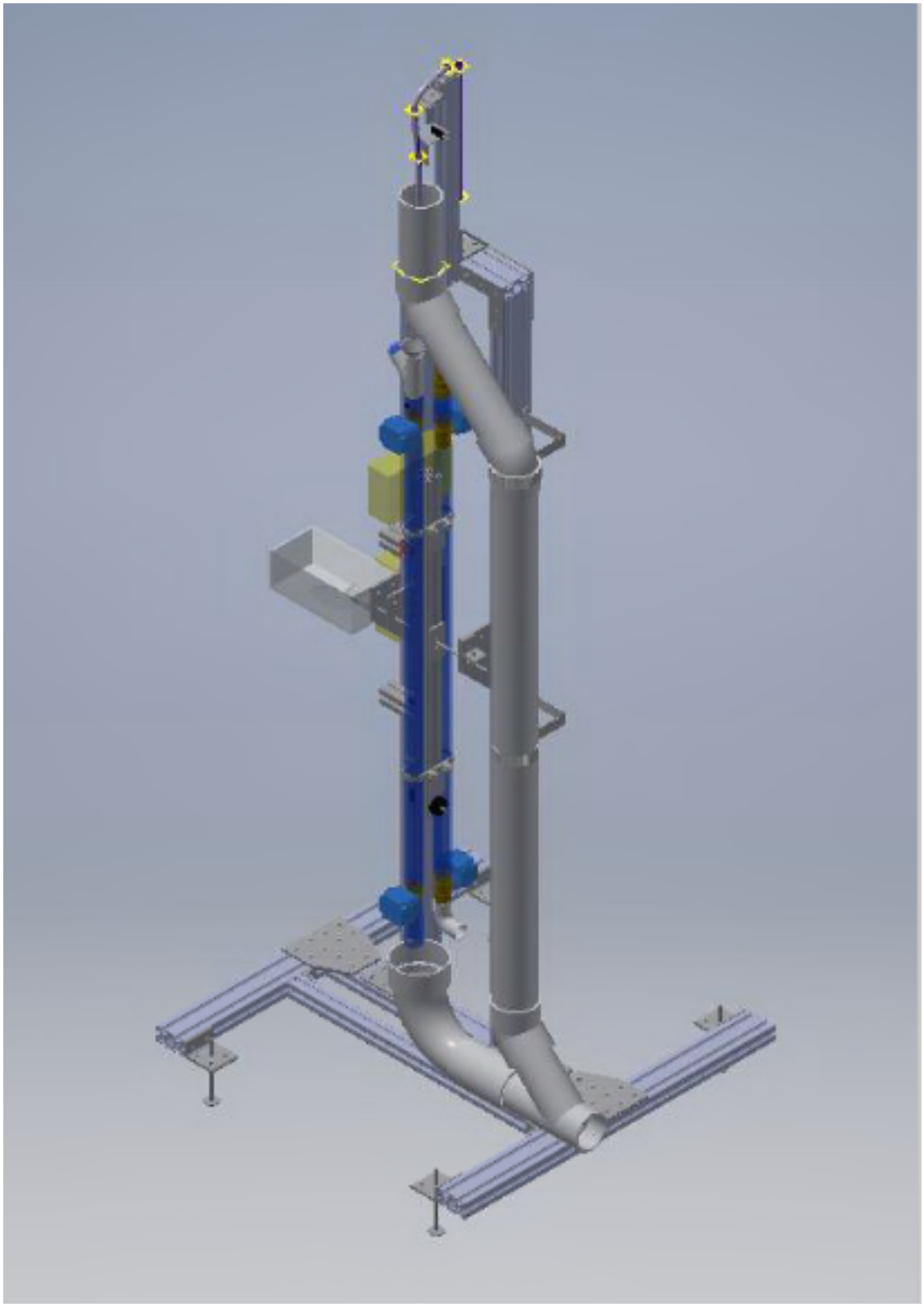

Figure 3.1. A three-dimensional rendering of the final overall design. To provide a sense of scale, the overall height of the assembled device is roughly 2.1 m (7 ft).

the 500 mA draw of other 1” valves considered. The Deelat valves have 1” National Pipe Taper (NPT) inlet and outlet, allowing them to be fastened at either end of the sample cylinder using 1” schedule 40 male NPT adaptors. Figure 3.2 shows front and side view profiles of the column assembly.

Because it rotates, the column assembly cannot have firm attachments on either end. This means that the water entering and discharging from the sample column must do so under gravitational flow. To aid in routing the water, an additional 1” schedule 40 male NPT adaptor threads above the Fill valve, connected in turn to 76.2 mm (3 in.) of 1” clear PVC, onto which is connected a 1” schedule 40 PVC wye. An 11-mm (3/8 in.) hole drilled in one side of the 76.2 mm (3 in.) PVC segment allows the tapping of a M12 x 1 hole for mounting a Honeywell LLE Series liquid level sensor.

A plastic funnel glued into the top end of the wye directs the water flowing from a ¾” schedule 40 PVC pipe extending from the water diverter (described below) into the sample column. There is a 2.54 cm (1 in.) gap between the end of the ¾” PVC and the 76.2 mm (3 in.) diameter top of the funnel. A 76.2 mm (3 in.) segment of 1” PVC pipe is glued to the second (angled) arm of the schedule 40 wye, and is capped on the other end. Once sample water reaches the liquid level sensor, the Fill valve closes and the inflow water routes to the discharge system. As the column unit rotates, any remaining water in the 1” segment above the Fill valve pours into the capped angle arm of the wye to prevent it from simply spilling out and affecting components below.

Another 1” schedule 40 male NPT adaptor and a 127 mm (5 in.) piece of schedule 40 clear PVC below the Drain valve route water leaving the sample column to the discharge assembly described below.

Like the sample cylinder, the reference cylinder contains motorized ball valves on either end of the PVC cylinder. However, because the reference cylinder only contains distilled water and does not need to pass sediment, the valves need not be the same diameter as the PVC cylinder. It is critical that the valves open large enough that a meniscus does not form across the valve, so that the reference cylinder vents completely to the atmosphere. A series of simple lab tests revealed that water menisci form across vertical pipe diameters smaller than 9.5 mm ($^3/_8$ in.). To prevent water menisci from forming, the reference cylinder uses ½” 12V Deelat DC Motorized SS304 ball valves, which have ½” NPT inlet and outlet. These valves are mounted to the 1” schedule 40 clear PVC reference column using 1” x ½” PVC schedule 40 bushings and ½” close brass nipples. The two Reservoir valves on the top of the reference column are connected with a 3” x ½” schedule 40 clear PVC pipe nipple, which forms the “reservoir” of distilled water previously described. An additional ½” close brass nipple and ½” schedule 40 PVC threaded elbow above the Vent valve prevent water from dripping into the reference cylinder while the valve is open during sampling. To ensure that both the sample and reference columns rotate at the same time during the sampling process, the PVC cylinders mount to either side of a 762 mm (30 in.) segment of 38.1 x 38.1 mm (1.5 x 1.5 in.)15 series 80/20 aluminum strut.

Four mounting plates bolted at each end of the slotted 80/20 frame, orthogonal to the PVC cylinders, make the physical connection between the cylinder unit and the rotating shaft. Electronic files provided to the committee members contain the technical drawings for the mounting plates. The 38.1 mm (1.5in.) spacing between cylinders allows for adequate room to

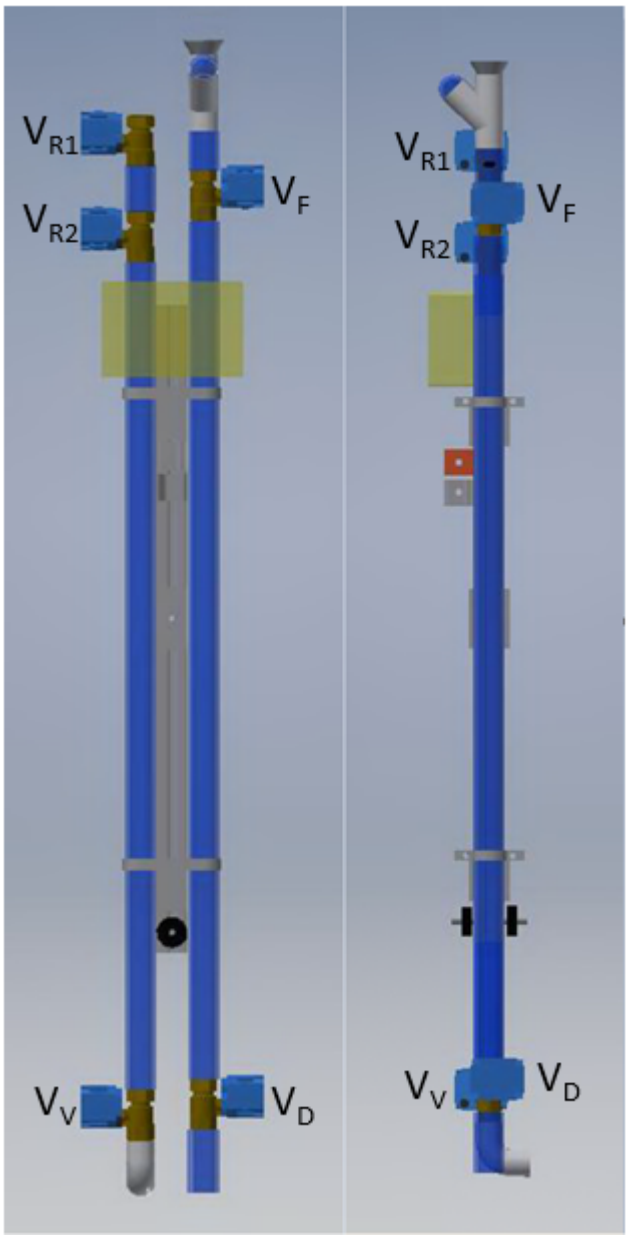

Figure 3.2. A rendering of the cylinder unit. The image on the left is a front view, with the Reference column on the left and the Sample column on the right. The image on the right represents a side view from the Sample cylinder side. V_{R1} and V_{R2} are the Top and Bottom Reservoir valves on the reference cylinder. The Vent valve on the reference cylinder is V_V. The Fill valve and the Drain valve on the sample cylinder are V_F and V_D, respectively.

mount the Deelat motorized ball valves on either end of the sample and reference cylinders. It also provides space to mount the cylinder to a 6 mm stainless steel rod as a rotation axle, supported by the surrounding frame and connected to the shaft of the gear motor. A through-hole drilled at the geometric center of the 80/20 mounting plate orthogonal to the PVC cylinders allows the stainless steel axle to pass through the 80/20 member and suspend the cylinder unit between the vertical members of the surrounding frame. The cylinder unit connects to the stainless steel axle via two set screw mounting hubs attached to additional mounting plates, bolted to the 80/20 member at its geometric center and orthogonal to the PVC cylinders. Electronic files provided to the committee members contain the technical drawings for the hub mounting plates. Furthermore, an electronics box as well as balance weights mount along the slotted frame of the 80/20 member, orthogonal to the cylinders. The balance weights were sized such that the entire cylinder unit (with both columns full of water) was balanced as well as possible about the axle, minimizing the torque exerted by the flipping motor.

Stand

An external frame supports the cylinder unit as well as the other components comprising the design. The frame material for this design is 80/20 T-slot aluminum. T-slot aluminum has a high strength-to-weight ratio and is very modular, making it an ideal prototyping framing option. The T-slot design allows connections to be made anywhere along the profile, providing an infinite number of mounting locations and allowing the design to evolve as needed. The cylinder unit dimensions mean that the stand's vertical members must be tall enough to allow rotation of the cylinder unit, while providing enough mounting room for the water diverter above and the discharge system below the cylinder unit. The weight and dimensions of the cylinder unit also require that the stand provides a strong and stable base. When the cylinder unit rotates, it exerts a moment on the stand about the axle. To provide stability and a reactionary moment to the flip, the two members forming the base of the stand extend out from the vertical members in the direction of the flipping moment. Rigid connections between the 80/20 members made by a variety of different 80/20 joining plates and corner brackets give the stand added strength and rigidity. Four adjustable feet allow for levelling the stand. Additionally, the feet elevate the base of the stand such that a discharge basin can integrate into the system. Figure 3.3 shows a front and side view of the stand.

Water Diverter

The sediment analysis device must recognize when a runoff event is taking place and whether the event is significant enough to sample. The parameters of this project assume that some source (either pump or gravity) supplies runoff to the design through an inlet tube. Furthermore, it is assumed that this sampling device does not have any control over the pump, nor does it receive any electronic signal that the pump is running. Thus, the system must determine whether runoff is being pumped based on its ability to sense flow coming out of the ½" inlet tube. This is done via a water diverter attached to the 80/20 frame above the sample and reference cylinders. Figures 3.4 and 3.5 depict the water diverter and its components. The diverter directs the incoming flow to either the sample cylinder or a discharge pipe, as controlled by a HiTEC HS-82MG MICRO servo motor. This servo is controlled by a system Teensy 3.2 microcontroller, which receives a signal from a flat plate flow sensor mounted on the lever arm

Figure 3.3. A rendering of the stand. The image on the left is a front view of the stand while the image on the right represents a side view.

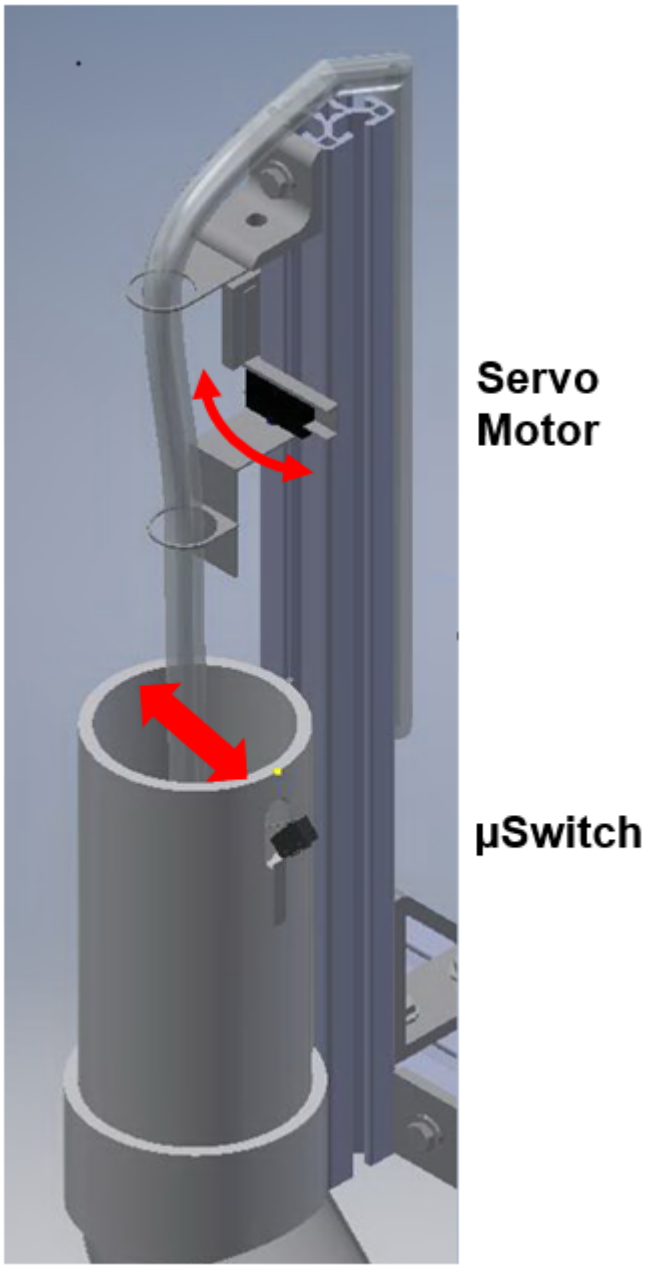

Figure 3.4. A three-dimensional rendering of the assembled water diverter from an upper/side view. The image shows the 3" thin-wall PVC diverter body, the 3" 45^{o} PVC elbow connected to the bottom of the body, the microswitch (lower black unit labeled "µSwitch") mounted on the outside of the body with its moment arm extending inside, and the inlet tube connected to an arm on the servo (upper black unit labeled "Servo Motor") and hanging down into the diverter body. As the servo rotates, it moves the inlet tube from the normal discharge position to over the ¾" PVC pass-through pipe, which is not visible in this view. The red arrow represents the movement path of the flexible tubing.

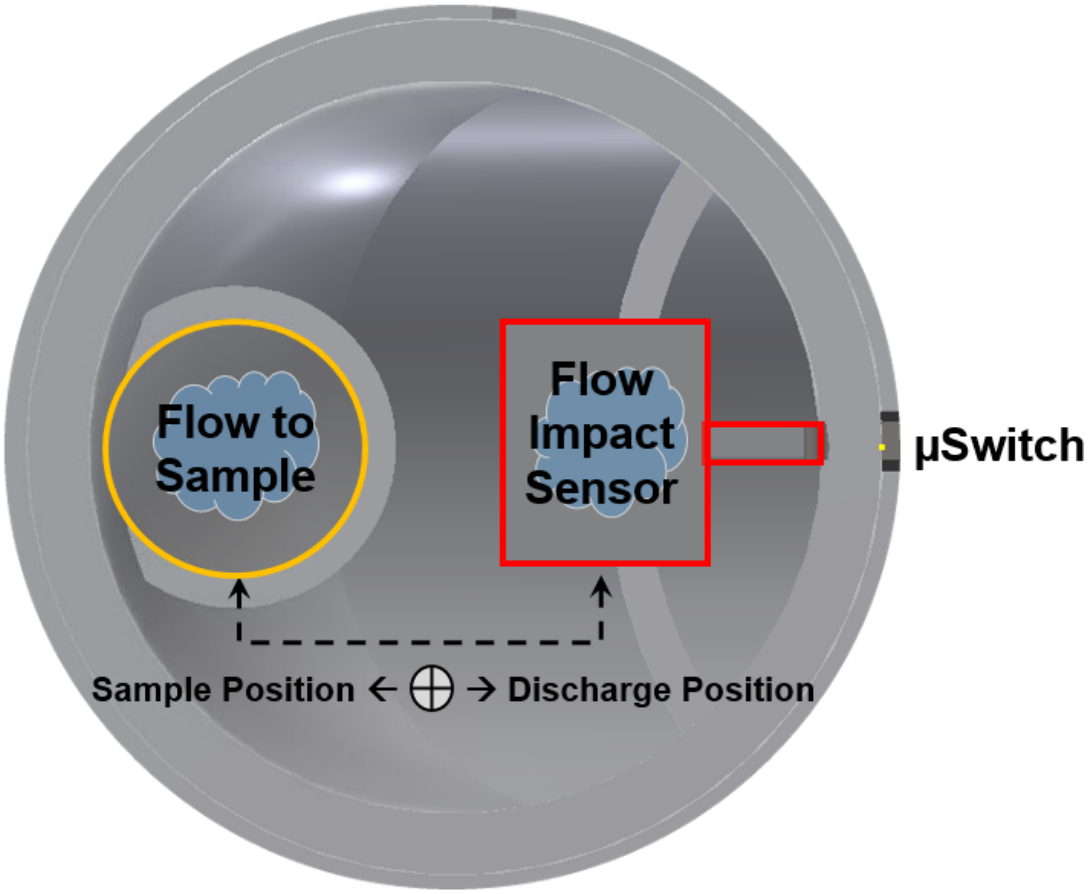

Figure 3.5. A rendering of the water diverter from above, looking directly down into the diverter. The image shows the outer 3" thin-wall PVC diverter body and the 3" 45° PVC elbow below it, the ¾" PVC pass-through pipe (outlined in yellow) that extends down through the elbow to carry water to the Sample column, the Honeywell microswitch in black to the right side, and the moment arm and flow sensing weight/plate (outlined in red) at the end of the moment arm. Before sampling, the servo holds the inlet tube to the right above the flow sensor in the "Discharge Position". When flow occurs the water pushes down on the weight/plate sufficiently to trigger the microswitch. The microcontroller then causes the servo to rotate, moving the inlet tube left over the ¾" pass-through pipe ("Sample Position") and directing its flow into the Sample column.

connected to a Honeywell Miniature Snap Action SPDT microswitch. This switch is normally open, but when flow from the inlet tube hits the flat plate and depresses the lever arm, the switch closes and sends a signal to the microcontroller, directing the servo motor to move the diverter arm (and thus the flow from the inlet tube) from discharge to sampling mode. Once the sample cylinder fills, the servo motor receives a signal from the microcontroller to return the inflow tube to discharge mode. If the inflow tube is still flowing at the end of the sample cycle, the flat plate and lever arm again trigger the microswitch, triggering a new sampling cycle as soon as the current cycle is completed.

Structurally, the HiTEC servo mounts to a vertical 80/20 member so that it is directly above a 305 mm (12 in.) length of 3" PVC thin-wall sewer pipe also bolted vertically to the 80/20 member. A 45° thin-wall 3" PVC elbow connects to the bottom of the 3" pipe to direct discharge flow to the discharge system described below. A through-hole drilled in the 45° elbow allows a 254 mm (10 in.) segment of ¾" schedule 40 PVC pipe to be glued to the inside of the 3" pipe while passing vertically through the elbow. This ¾" PVC pass-through pipe is positioned directly above the sample cylinder. When the servo diverts the inlet tube, it moves the flow from the larger 3" discharge pipe to directly over the ¾" pass-through pipe, thus diverting the flow into the sampling funnel and from that into the sample column.

The Honeywell microswitch flow sensor mounts to the outside of the 3" PVC, minimizing the risk of water harming the sensor. A through hole drilled in the 3" PVC allows the micro-switch's 50 mm (2 in.) moment arm to extend into the center of the pipe. A 2.54 x 2.54 cm (1 x 1 in.) flat weight attaches to the end of the micro-switch moment arm. For the micro-switch to close, a force of 0.9 N must be applied to a button on the switch. This weight added to the moment arm pre-loads the button, ensuring that the microswitch is sensitive enough to indicate flow by triggering the microswitch at the expected pump rate of 5.7 L min^{-1} (1.5 gpm).

The flexible ½" tube coming from the pump is fastened to the top of the 80/20 vertical member and directs flow down into the 3" thin-wall PVC. The end of the tube passes tightly through a sheet-metal arm connected to the servo motor. The servo arm initially positions over the 2.54 x 2.54 cm (1 x 1 in.) flat weight connected to the microswitch's moment arm. Thus, all runoff coming from the pump impacts the weight and is discharged via the 3" 45° elbow. If the flowrate coming out of the tubing is greater than or equal to 5.7 L min^{-1} (1.5 gpm), the button on the microswitch is depressed. This closes the switch and triggers an interrupt on the Teensy 3.2 digital input line, signifying that the system should begin the sampling process.

Inlet and Discharge System

For lab testing purposes, the design incorporates both a pump for supplying water or a water-sediment mixture to the sediment analysis device, and a pump for transporting the discharged sediment-water mixture to a floor drain in the lab. To meet the desired inlet flowrate of 5.7 L min^{-1} (1.5 gpm), a 1/10-horsepower Wayne Utility Pump pumps the water or water-sediment mixture from a 13.5 L (3.5 gal) shallow storage bin to the top of the system's water divider roughly 2.1 m (7 ft) above the floor. The pump is capable of emptying the bin down to a depth of 3 mm, producing a continuous supply of inlet water to the sediment analysis device until the bin is almost drained.A discharge system integrated into the sediment analysis device routes both the diverted water from the water diverter and the sampled sediment-water mixture into another 13.5 L (3.5 gal) shallow storage bin. Figure 3.6 shows the discharge system

Figure 3.6. Rendering of the discharge system. The image on the left is a front view of the discharge system mounted to the stand, while the image on the right is a side view. Not shown is the 4” x 3” PVC closet bend, which is used to catch the flow leaving the Sample column and direct it into the discharge piping. This bend is connected to the lower branch of this 3” thin-wall PVC sewer pipe using a 3” flexible rubber coupling.

mounted to the stand. Segments and fittings of 3" thin-wall PVC sewer pipe make up the discharge system that moves the water into a discharge bin. The pipe and fittings are mounted to the 80/20 stand in several locations using plumbers' strap.

To capture the flow coming out of the sample cylinder, a PVC-DWV 4" x 3" closet bend elbow mounts to a frame member directly below the Drain Valve. The closet elbow mounts to the base of the 80/20 stand, centering the 4" hub underneath the Drain Valve so offering a large opening to collect the outflow. The 3" thin-wall sewer pipe used for the rest of the discharge system has an outside diameter smaller than the inside diameter of the DWV closet elbow's 3" hub, so a 3" flexible rubber coupling joins the two. The exiting flow from both the water diverter and the sample cylinder merge together in a wye, and the combined flow flushes into the discharge bin. The design of the stand and its supporting feet is such that the exiting flow is 12.7 cm (5 in.) above ground level, allowing the discharged flow to pour out of the wye and into a discharge bin.

Rotation

As mentioned in the previous section, sediment begins to settle on the bottom of the sample cylinder once the incoming sample reaches a semi-quiescent state. The system must invert such that the settled particles re-suspend within the column while the pressure reading is taken. A 32 rpm ActoRobotics HD Premium Planetary Gear Motor inverts the cylinder unit 180˚. The gear motor was selected to provide sufficient torque (21 N m) such that the cylinder unit rotates in 4 s. Appendix A shows moment of inertia calculations used to determine the torque required to rotate the cylinder unit. The motor has a Hall Effect encoder providing the relative position of the output shaft. To rotate the system, the gear motor mounts to an 80/20 90-degree angled flat plate such that its torsional load is imparted to the axle at the cylinder unit's center of mass. Drawings contained in the electronic files provided to the committee members show modifications to the plate that allow the gear motor to rigidly mount to the stand. A HB-25 motor controller drives the motor, in turn controlled by a signal from the microcontroller. A plastic enclosure mounted to the same plate as the gear motor houses both the motor and the motor controller. Figure 3.7 shows the enclosure and mounting of the gear motor.

The motor output shaft and the cylinder unit axle are both 6 mm diameter, so a 6 mm x 6 mm steel clamping shaft coupling connects the output shaft to the 6-mm stainless steel axle supporting the cylinder unit. Two 80/20 90-degree angled flat plates bear the load of the rod and thus the weight of the cylinder unit. Four 6 mm flanged ball bearings pressed into the plates reduce the rotational friction of the stainless steel axle. Because rotation is in one plane, the ball bearings do not have to withstand axial loads. Two set screw hubs transfer the torsional load imparted by the motor to the cylinder unit. Dimples drilled into the stainless steel axle allow the set screws to create a solid connection between the axle and the cylinder unit.

An additional set-screw mounting hub attaches a non-transparent, 76 mm (3 in.) plastic disc to the end of the stainless steel axle opposite the gear motor. A photogate used in conjunction with the plastic disc provides an additional means of determining the position of the flipping arm as it rotates. The plastic disc has a 3.2 mm (1/8 in.) through hole drilled near the perimeter of the disc. As the stainless steel axle rotates, the disc rotates between the two sides of the photogate. The photogate detects whether the cylinder unit is in the fill position or not based The photogate mounts to a printed circuit board (PCB) fixed to one of the 80/20 uprights. Figure

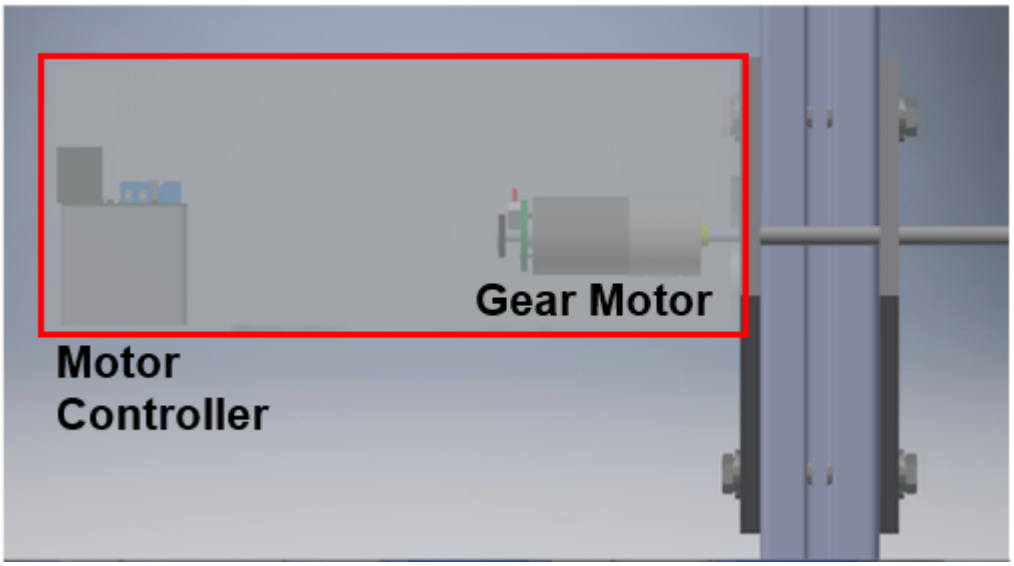

Figure 3.7. Rendering of how the gear motor and motor controller mount to the stand. The image is a front view of the mounting and illustrates the clear plastic enclosure surrounding the motor and the controller (enclosure outlined in red).

3.8 depicts the mounting of the photogate and the disc.

To ensure that the cylinder unit is held vertically in both the filling and inverted positions, two magnetic cabinet latches (shown in Figure 3.9) hold the unit in place after rotation. These latches are mounted on two 127 mm (5 in.) 80/20 members fastened horizontally to the vertical stand upright, with one on either side of the axis of rotation. Magnetic strips glued to two 80/20 inside corner brackets mounted on the cylinder unit create contacts for the latches.

Sediment Analysis

Instrumentation

The design components enable the system to obtain a precise sample volume, and must also allow the system to capture a differential pressure measurement via a differential pressure transducer. The selection of the differential pressure transducer is dependent on the expected differential pressure range between the two columns. As mentioned earlier, the change in net density due to added sediment causes the differential pressure between the two columns, and the sediment concentrations in runoff to vary based on several parameters, including land practice. Because this system must operate at construction sites where the sediment load in runoff can be high, it is critical to establish the range over which the system must measure. Based on a study by Hayes et al. (2005), 130,000 mg L^{-1} is typically the highest sediment concentration contained within runoff leaving a construction site. Based on this and as stated in the Design Objectives, this system therefore needs to measure sediment mass in a water sample across the range of concentrations from 1,200 mg L^{-1} to 120,000 mg L^{-1}. Although the minimum detectable concentration is theoretically equal to the minimum resolution at which the system's differential pressure transducer can sense, this study chose to measure sediment concentrations over these three orders of magnitude. This means that at the system's sample volume of 490 mL, the low concentration of 1,200 mg L^{-1} is the equivalent of 0.59 g of sediment while the high concentration (120,000 mg L^{-1}) equals 59 g. To further put this in perspective, 0.59 g is the mass of approximately 40 grains of 2 mm sand.

With the concentration range established, the next step in the design process is to select a differential pressure transducer matching that full-scale range. Using the physical dimensions of the reference and sample cylinders as well as the maximum sediment concentration, a simple calculation (see Appendix B) determines the maximum differential pressure seen between the two columns, which turns out to be approximately 0.56 kPa (2.25 in. H_2O). After examining multiple differential pressure sensors that measure this pressure range, this design uses a Honeywell RSC Series RSCDRRI002NDSE3 pressure sensor, thought to provide the best combination of precision, ease of use, and low cost. This sensor's ports are 1.53 mm in diameter, and they can only be used to read gas pressures (no liquid contact). Since we are dealing with measuring pressures in liquids other liquid-liquid sensors were also examined, but the most sensitive of those had a 14 kPa (55 in. H_2O) full-scale reading, not providing sufficient sensitivity. The selected RSC sensor has a listed accuracy of ±0.1%, and outputs a temperature compensated 24-bit digital signal. Furthermore, the RSC sensor has a low power draw of less than 10mW operating at 3.3 Vdc, and it transmits the data via a Serial Peripheral Interface (SPI).

Selecting the RSC sensor then allows for the selection of the other electronic components. Not only is the collection and storage of the pressure data important, but the overall

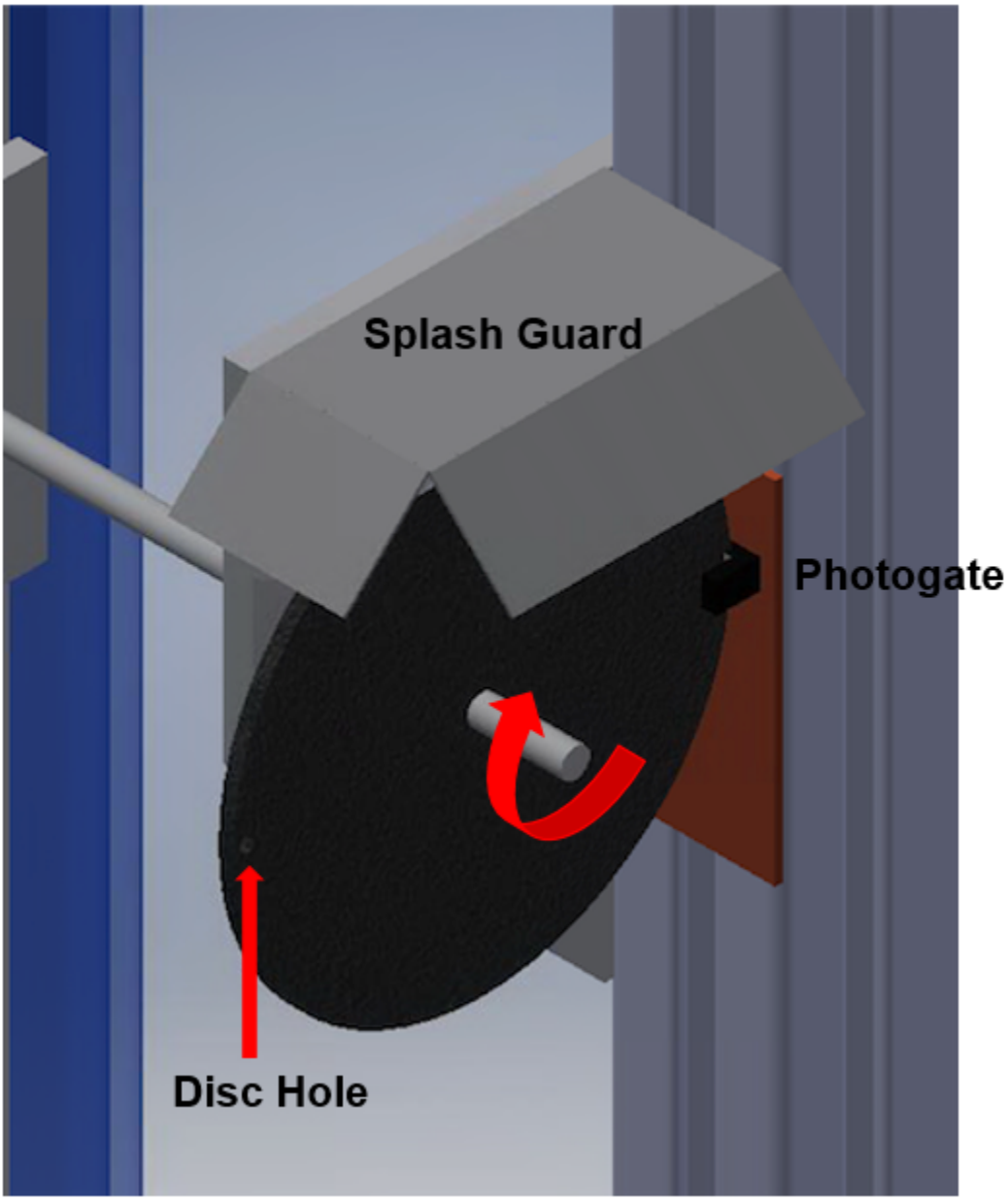

Figure 3.8. Three-dimensional rendering of the photogate and disc used for column unit positioning. As the motor rotates the cylinder unit, the black disc also rotates. The orange PCB in the drawing mounts to the vertical member of the 80/20 stand. The photogate solders to the PCB such that the disc rotates between the photogate. The cylinder unit is in the fill position when the through hole in the disc allows the light emitted by the photodiode to pass through the hole. The gray sheet metal plate above the disc and PCB protects the photogate from any splashing water.

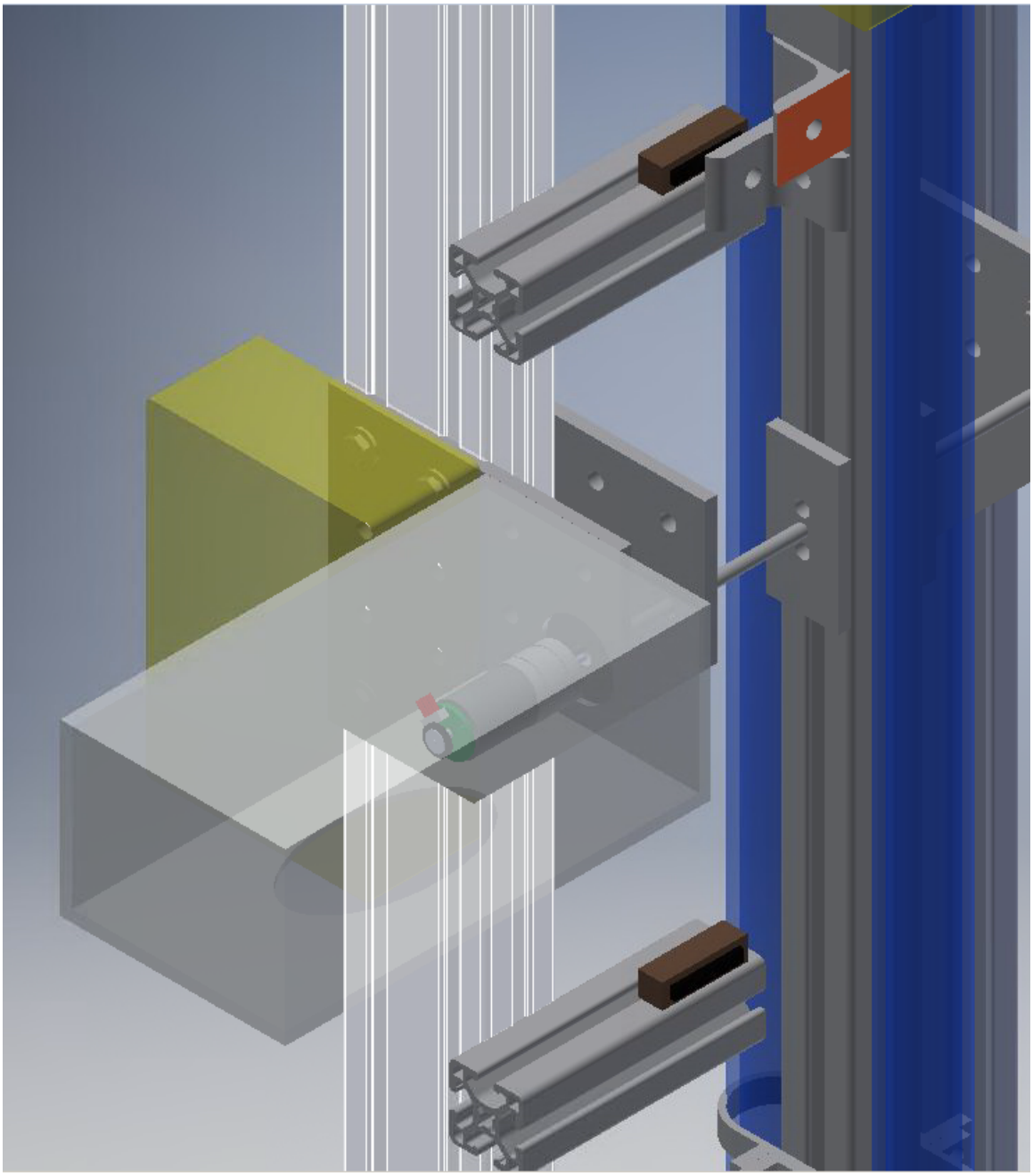

Figure 3.9. Three-dimensional rendering of the magnetic latches, represented by the brown boxes. The orange element in the upper right corner of the rendering represents the magnetic strip mounted to the right arm of the cylinder unit. When the cylinder unit is rotated 180^{o} about its axle, this strip will contact the lower magnetic latch, providing a solid connection.

process control is critical to the system being able to collect that data autonomously. This process entails opening/closing the motorized ball valves, operating the motor and servo, as well as receiving inputs from the water diverter and the liquid level sensor (see Appendix C). A PJRC Teensy 3.2 microcontroller was selected to manage the data collection and system control processes. The Teensy 3.2 operates at 3.3 Vdc with a processor speed of 72 MHz. Additionally, it provides 13 digital input/output pins (23 if all 10 analog pins are used as digital pins) that are 5 V tolerant, allowing it to interface with 3.3 V and 5 V signals.

After carefully analyzing the overall system design and mapping the wiring between the Teensy 3.2 and the different devices, a second Teensy 3.2 microcontroller was added to the system to provide additional digital input pins while minimizing the number of wires running between the stand and the moving cylinder unit. In this design, one of the microcontrollers acts as the primary controller while the other operates as the secondary. The primary microcontroller has unidirectional control and sends serial commands to the secondary controller, instructing it when to perform each task. The secondary controller communicates back to the primary via the same serial lines. In this setup, each microcontroller is responsible for executing tasks related to the electrical components it controls. Each microcontroller is soldered onto a PCB containing various components used to execute the different system operations. A general breakdown of the two microcontrollers' responsibilities is shown in Figures 3.10 and 3.11.

In addition to communicating with the secondary microcontroller, the primary controller is responsible for reading the pressure data sent by the secondary Teensy and writing that data in the form of non-volatile memory. A 3.3 V Sparkfun Level Shifting microSD Breakout stores the data on a 16 GB microSD card. The Teensy reads and writes the pressure data to the microSD via SPI. Furthermore, because the system is likely to be implemented in remote locations, it should be able to wirelessly transmit the stored pressure data. There are several wireless transmission techniques available, with each having advantages and disadvantages. This system's design accommodates both WiFi and radio transmission, such that the operator could use whichever method is better suited for their setup. The PCB housing the main microcontroller provides an interface for either a 3.3 V ESP8266 WiFi module or a 3.3 V 2.4 GHz XBee radio. These devices provide similar transmission range, with the XBee radio delivering this at the lower energy requirement of 30 mA versus the ESP8266 demand of 80 mA. However, when not limited by the processor speed, the ESP8266 allows higher transmission speed. The microcontroller reads the data stored on the microSD and writes it to the XBee/ESP8266 via serial communication.

In addition to data storage and transmission, the primary microcontroller interfaces with the 32-rpm gear motor used to rotate the cylinder unit. The Parallax HB-25 motor controller interprets a pulse width modulated (PWM) signal coming from the Teensy and sets the motor direction via an H-bridge. The motor controller modulates its 12 V output to alter gear motor speed. Furthermore, the primary microcontroller uses two of its input lines as interrupt lines such that it can read the pulses coming from the two output lines on the motor encoder. The Hall effect encoder operates at 5 V with the output lines 90° out of phase. The microcontroller interprets the phase relationship between the two encoder signal lines to determine whether the motor is turning clockwise or counter-clockwise. It also counts the pulses such that it can obtain a relative position of the motor output shaft, with the encoder providing 12,659 countable events per revolution.

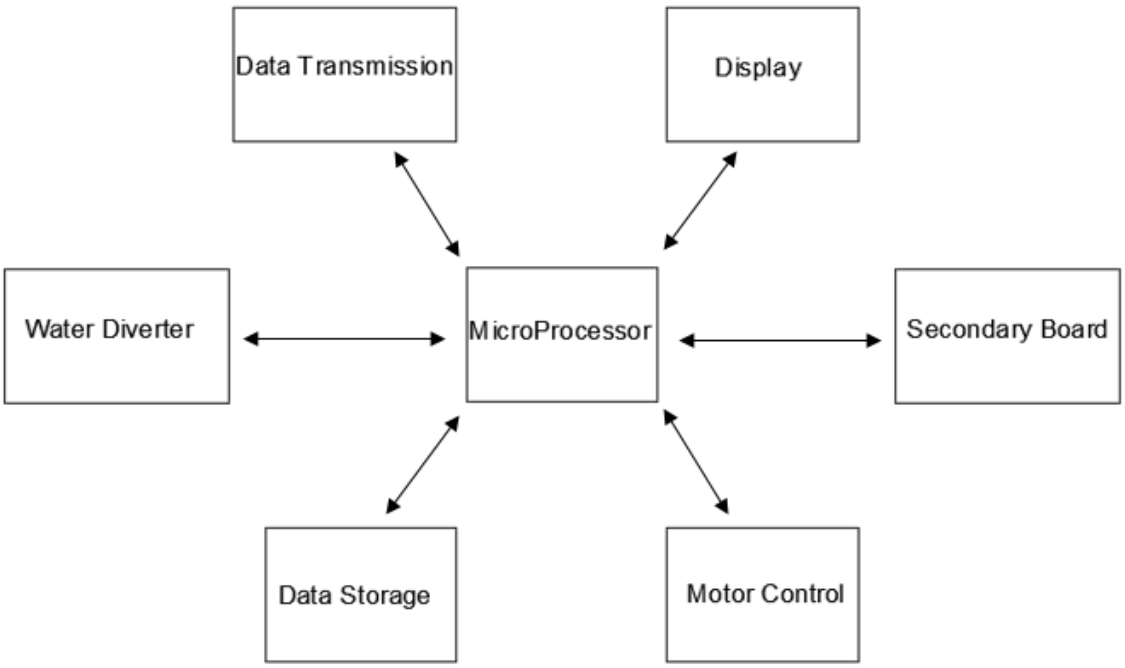

Figure 3.10. The general responsibilities of the main electronics box. The primary Teensy 3.2 in this box communicates with the secondary Teensy (on the Secondary Board) and controls its operations. Additionally, the primary Teensy is responsible for controlling the flipping motor, reading the motor encoder, responding to the diverter flow sensor and operating the water diverter, storing/transmitting the pressure data, and turning on/off an RGB LED.

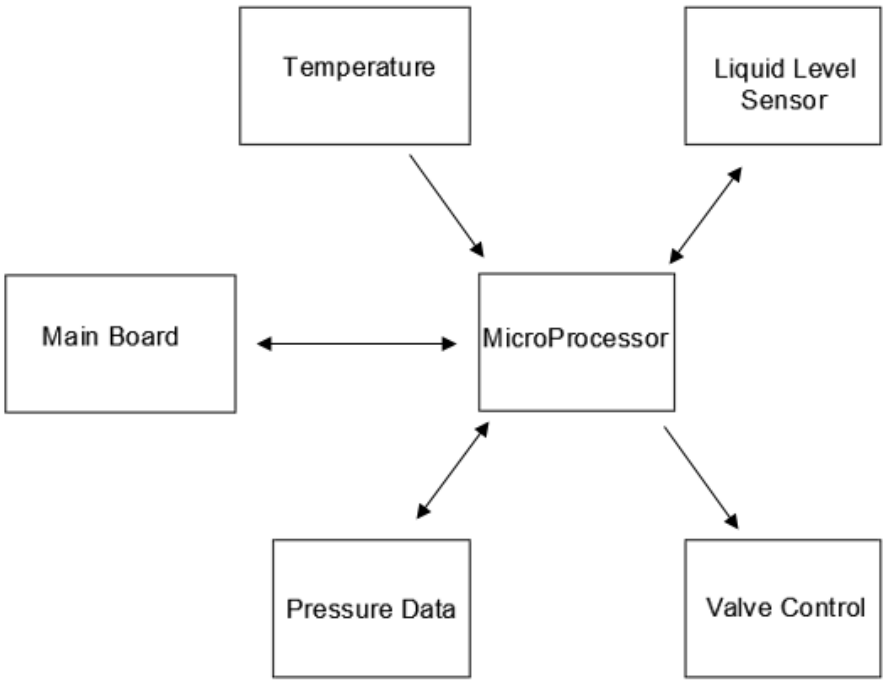

Figure 3.11. The general responsibilities of the secondary electronics box. The secondary Teensy 3.2 in this box communicates with the primary Teensy in the main box, operates the valves, and receives inputs from the differential pressure transducer, liquid-level sensor, and thermistors.

Quadrature encoders such as this one require a baseline index to count from. Because the cylinder unit rotates 180° from a defined location, the relative encoder works well for this application. However, if the system experienced a power outage during rotation or if the cylinder unit did not begin the sampling process in the correct orientation, the relative encoder has no way of adjusting for this. Thus, a 5 V Sparkfun photogate actively senses the orientation of the cylinder unit. When the cylinder unit is in the fill position, the photo gate outputs a digital signal of logic 1 (or High). Therefore, during rotation, the microcontroller can use the quadrature encoder outputs to increment or decrement a counter relative to the index position. Furthermore, if the system were to lose power during operation, it can look at the photogate signal on power up to determine if the cylinder unit is oriented correctly. If it is out of position, the primary Teensy can rotate the motor in the counter-clockwise direction until the photogate output line goes High.

The primary Teensy is also responsible for operating the water diverter servo. A PWM digital output line on the microcontroller positions the HiTec servo arm. The HiTec servo operates on 5 V, but it accepts a pulse amplitude from 3-5 V, allowing the servo to be controlled by the Teensy's 3.3 V digital output line. Additionally, the primary microcontroller uses the Honeywell microswitch on the water diverter as an input to determine whether a sample is flowing to the system. The switch is normally open, meaning that an internal pullup-resistor drags the digital input line High when the switch is not depressed. However, when the incoming flow depresses the lever arm and closes the switch, the input line goes Low. The input line coming from the water diverter switch is set as an interrupt line to both the primary and secondary Teensy controllers. This allows the system to enter a low-power state when flow is not present, thereby conserving energy. Finally, the primary Teensy controls a LED-RGB 5 mm Square Piranha. The three output lines going to the Piranha allows the Teensy to turn on and off red, green, and blue LEDs. This component provides the operator with a visual indicator of current system state. The schematic and the board layout for the primary PCB are shown in Appendix D and Appendix E.

As seen in Figure 3.3, the secondary microcontroller has several responsibilities including overseeing the opening/closing of the valves. Each of the five Deelat motorized ball valves operates at 12 V and pulls approximately 150 mA during the 8-10 s required to open or close the valve. The wiring scheme for the valves is that of a three-wire, ON/OFF design. The control line determines whether the valve is open (if the line is tied to 12 V) or closed (if the line is tied to GND or open). The secondary Teensy performs this valve control by sending a digital signal to the base of four TIP 120 Darlington transistors, which tie the valve control lines to either 12 V or GND.

The secondary microcontroller also collects readings from the Honeywell RSC differential pressure transducer. The Honeywell sensor itself is directly mounted on the secondary PCB, and the pressure transducer ports are connected to the sample and reference cylinders using Cole Parmer C-Flex Clear Tubing. A ¼" United States Plastic (USP) Corporation threaded adapter is threaded into the reference and sample cylinders approximately 7.5 cm (3 in.) above the top of the Vent and Drain valves. The adapters thread into a 6.35 (¼" in.) NPT hole tapped directly into the clear PVC sample and reference cylinders. A 6.35 x 1.6 mm (¼ x 1/16 in). USP reduction coupler reduces the 6.35 mm (¼ in.) C-Flex tubing coming from the 6.35 mm (¼ in.) threaded adapter to 1.6 mm (1/16 in.) C-Flex tubing such that it tightly connects to the

barbs on the Honeywell pressure sensor.

As the cylinder is filled, the water tries to move from the cylinder into the adapter and C-Flex tubing, compressing the air in the tube and transferring the pressure caused by the height and density of the liquid in the cylinder to the pressure transducer. As the water moves into the adapter and tube, a meniscus forms at the air-water interface. Using a larger inner diameter for the adapter and tubing where the meniscus forms reduces the effect of the meniscal force on the pressure reading, thus leading to a more accurate measurement (see Appendix F). As mentioned previously, the secondary Teensy communicates with the pressure transducer via SPI. During sampling, the secondary Teensy reads a temperature and pressure measurement from the sensor. It then serially writes the respective 16-bit and 24-bit values to the primary Teensy once every 100 ms.

The secondary Teensy is also responsible for reading the digital output line coming from the Honeywell LLE Series liquid level sensor. This sensor operates on 5 V and has a current draw of 15 mA. The liquid level sensor actively determines whether the water level in the sample cylinder is above the Fill valve. During the filling process, the secondary Teensy verifies when the sample column is full by reading when the liquid level sensor's digital output line goes from High to Low. When this transition occurs, the secondary Teensy sends a serial command to the primary Teensy, instructing it to move the servo arm, routing the incoming flow to discharge.

Additionally, the secondary Teensy reads two analog input lines from thermistors placed on the sample and reference cylinders. Each thermistor outputs a signal corresponding to the water temperature in each of the respective columns. Although a change in water temperature results in a small change in density, water temperature does have a significant effect on viscosity. Adding thermistors to the design is primarily for future research involving sediment size distribution. The schematic as well and the board layout for the secondary PCB are shown in Appendix G and Appendix H.

It is important that the PCBs fit neatly into a self-contained package that prevents environmental damage. A Bud Industries BT-2724 171 x 121 x 55 mm (6.7 x 4.8 x 2.2 in.) NEMA 4 enclosure mounted adjacent to the gear motor on the stand houses the primary controller PCB. The same weather resistant enclosure type houses the secondary PCB and mounts to the 80/20 cylinder unit above the Vent and Drain valves. Through-wall connectors threaded into 15.9 mm (5/8 in.) NPT holes tapped along the sides of the enclosures allow the wiring for the various electrical components to pass through the sides of the enclosure and insert into screw terminals. Additionally, Molex power connectors soldered on the PCBs provide mounting locations for the 12 V, GND, and serial communication wires to connect between the two boards.

Power

The system may operate autonomously in a remote location. Thus, it must draw energy from an independent power source. Because a runoff event can last for hours or days, the power supply must be large enough to provide continuous power over the event duration. However, as a realistic design constraint, the energy source for this system should allow continuous operation for three days. To choose an energy source capable of this, the power demand for the entire system must be determined. A preliminary energy budget based on each component's current draw (via the component's datasheet) indicated that when collecting and analyzing a sample

once every minute, the total energy consumption for three continuous days of sampling summed to 120 A-hrs. However, operation of the actual system defined the true sampling rate and energy demand, and later chapters discuss this testing and results. For testing purposes, a TENMA Laboratory DC Power Supply supplied the power required to operate the design. A 2 A in-line fuse protected the electronics from pulling too much current and damaging the electronic devices. Furthermore, the primary and secondary PCBs each have both 5 V and 3.3 V voltage regulators to regulate the supplied 12 V down to the desired voltage level specific to each component.

CHAPTER FOUR
SYSTEM TESTING

Volume Testing

To get a precise pressure differential between sample and reference columns, it is critical that the system accurately measures total sample volume. Therefore, before subjecting the system to sediment testing, it first had to show it could repeatedly capture a constant volume of clean water. These initial volume tests used the same sample capturing process used for the other overall design tests, though the tests were done by hand. A TENMA Laboratory DC Power Supply generated the 150 mA required to operate each of the 12 V valves.

The test process began with closing the bottom ball valve and pouring distilled water through the open top valve until the water level rose above the valve, at which point the top valve was closed. To replicate the filling process used by the system, water was poured into the cylinder such that the column filled in around 5 s. After filling, the cylinder was then flipped to discard any water that had collected above the top valve.

A METTLER PM 4000 scale capable of measuring to 0.01 gram was then used to weigh each water sample. A dry bucket was tared on the scale, then the valves were opened to drain the water out of the PVC column and into the bucket. A Plexiglas shield box placed over the scale and bucket minimized the impact of air movement or other effects on the measured values. Once the scale captured a stable weight measurement, the bucket was emptied and dried. This process was repeated for a total of 10 replicates.

Preliminary Sediment Testing

Once the preliminary volume testing demonstrated that the system can capture a precise known volume, the next step was to determine how accurately the system can measure sediment mass. Preliminary sediment tests with the system design allowed verification as to whether the components selected can provide a sufficiently accurate and repeatable sediment mass measurement. Table 4.1 shows the tested concentration values and size distributions. The chosen sediment size distributions for testing were classified as sand, silt loam, and clay loam. Fine sand was the base size distribution used for the most preliminary tests, as it is well-behaved in water and does not form large aggregates. Silt loam and clay loam soils provide additional insight as to how the system performs when subjected to real soil types. There are three replicates for each test, corresponding to a total of 27 tests.

Prior to testing, an environmental chamber was used to dry the sand, silt loam, and clay loam for 24 hrs at a temperature of 100°C, removing any moisture in the soil. For each test replicate, a tared plastic cup was used measure the dry sediment mass corresponding to the target concentration. A METTLER PM 4000 scale was used to tare the cup and weigh the sediment to the nearest 0.01g.

The sediment testing consists of operating the system as laid out previously in the design section. However, instead of using a pump to fill the sample column, the column was filled by

Table 4.1. Concentrations, size distributions, and masses used in the preliminary sediment testing. Each test consists of three replicates.

Preliminary Sediment Tests		
Target Concentration (mg L^{-1})	Tests	Target Mass (g)
1,000	Sand	0.5
4,000	Silt, Clay	2.0
10,000	Sand	5.0
50,000	Sand	25.0
80,000	Sand, Silt, Clay	40.0
100,000	Sand	50.0

hand-pouring clean water into the cylinder. Once the sample column was filled halfway with clean water, the sediment in the plastic cup was poured into a funnel placed above the Fill valve, injecting the sediment into the cylinder. Clean water was then used to fill the rest of the sample column, and the Fill valve was closed once the water level contacted the liquid level sensor. The scale was then used to again weigh the plastic cup after pouring out the sediment to provide a measure of any sediment sticking to the cup walls, allowing determination of the true amount of sediment added to the sample column. This process provides a known sediment mass added to the known volume of the sample cylinder. The rest of the sampling process was then completed as designed, with the differential pressure values stored on the microSD card. Each of the three replicates for each test followed this test sequence.

Final Sediment Testing

Proving successful design of the sediment concentration analysis device entails testing that it can autonomously and repeatedly detect sediment mass values for various concentrations within an established accuracy. The preliminary sediment testing established this repeatability and target accuracy. For the final sediment tests, the chosen concentration values were 1,200 mg L^{-1}, 12,000 mg L^{-1}, and 120,000 mg L^{-1}. To prove that the system can achieve this repeatability and accuracy for the range of sediment size distributions, test replicates were run at each concentration with sand, silt loam, and clay loam. There were three replicates for each test, corresponding to a total of 27 tests. Table 4.2 shows the target mass associated with each concentration and soil type used in the final sediment testing.

As with the preliminary sediment testing, the environmental chamber was used to dry the sand, silt loam, and clay loam for 24 hrs at a temperature of 100°C to remove moisture. A tared plastic cup held the sediment mass corresponding to the target concentration, using the METTLER PM 4000 scale to tare the cup and weigh the sediment.

The sample column was again filled by hand-pouring clean water into the cylinder. Once the sample column was filled halfway with clean water, the sediment in the plastic cup was poured into a funnel placed above the Fill valve, injecting the sediment into the cylinder. Clean water was the used to fill the rest of the sample column, and the Fill valve was closed once the water contacted the liquid level sensor. The scale was used to weigh the plastic cup after filling to determine the true amount of sediment added to the sample column. The rest of the sampling process continued as designed, with the differential pressure values stored on the microSD card.

Table 4.2. Concentrations, size distributions, and masses used in the final sediment testing. Each test consists of three replicates.

Final Sediment Tests		
Target Concentration (mg L^{-1})	Tests	Target Mass (g)
1,200	Sand, Silt, Clay	0.59
12,000	Sand, Silt, Clay	5.90
120,000	Sand, Silt, Clay	59.90

Each replicate followed this test sequence.

Operational Testing

As mentioned in the design section, the system relies on several different components successfully operating in sequence and sometimes simultaneously. Therefore, prior to running tests on system robustness, it was crucial to test each of the components individually as well as to verify that the system could in fact step through the sampling cycle without any human interaction. This testing was done using clean water, cycling it through the system using the inlet and discharge pumps; sensing flow via the Honeywell switch; diverting flow using the servo motor; filling the sample cylinder by opening/closing valves and reading the liquid-level sensor; flipping the cylinder unit in the clockwise direction by motor; reading the pressure transducer and writing to the microSD during sampling; rotating in the counter-clockwise direction via motor and photogate; and opening valves to flush the sample cylinder.

Once the system could do each of these operations in sequence, it then cycled continuously, representative of actual operation. As described in Chapter Three, control of these processes is done through the two Teensy 3.2 microcontrollers. The Arduino code uploaded to the Teensy's is included in the electronic files provided to the committee members.

Environmental Chamber Testing

It is essential that the system can function in conditions other than those of a controlled lab environment. Specifically, the design should operate across a range of temperatures similar to that seen in the field. Although extensive testing should be done with the system implemented in an outdoor environment, this test simulated a change in temperature by placing the design in an environmental control chamber, subjecting the device to a cold air temperature of 5°C and a warm air temperature of 40°C. The goal of this testing was to provide information on the following questions: 1) does the Honeywell RSC Series differential pressure transducer respond to heating and cooling, so does the temperature change affect the RCS's ability to accurately measure sediment mass?; 2) are other system elements negatively affected by either temperature extreme?; and 3) does changing the water temperature truly significantly affect the sediment fall velocity, as the settling theory says it should?

To answer these questions, the system was used for three replicates of a 12,000 mg L^{-1} sand test at 5°C and 40°C, for a total of 6 tests. The environmental chamber, with the sediment analysis device placed inside, was cooled/heated to the respective test temperature for 6 hrs before testing, allowing the entire system to reach the test temperature. Once the system reached

the target temperature, the testing proceeded identically to the preliminary and final sediment testing.

Robustness Testing

Having a system that regularly requires substantial maintenance is not sustainable. Therefore, a final robustness test was used to indicate how long the design can operate autonomously before one of the components fails. Conducting this test consisted of allowing the device to operate autonomously and continuously while observing when a component failed. The design of this test was such that a water sample containing 60,000 mg L^{-1} of silt loam was pumped from the supply bin to the water diverter. A discharge pump recirculated the sediment-water mixture from the discharge bin back to the supply bin. This closed system setup prevented the introduction of additional sediment to the system, and it guaranteed that the system had a continuous water supply. Note that because some of the sediment was able to settle within the basins this test was not used to determine the accuracy of sediment readings, but rather just to examine general device operation.

At the conclusion of testing, an XBee Pro radio transmitted the pressure data stored on the microSD to a receiving XBee radio attached to a computer, which was then used to analyze the data. This wireless transmission testing verified whether the design can reliably transmit data.

Finally, the robustness testing includes measuring the power consumption of the system as it operates. This testing was done by measuring the current draw of the system as it operated. An Extech Digital Clamp-On Ammeter was clamped around the supply wire running from the power supply to the system. The Ammeter read and digitally displayed the Root Mean Square (RMS) current passing through the supply wire at a resolution of 1 mA. The current draw for each stage of the sampling process (filling, rotating, sampling etc.) was manually recorded in a spreadsheet over three sampling cycles of about 90 seconds each.

CHAPTER FIVE
RESULTS AND DISCUSSION

Volume Testing

Table 5.1 shows the results from the volume repeatability testing. The calculated coefficient of variation across the 10 samples was 0.02% (200 mg L^{-1}). The volume test results show that the valve-column design can repeatedly capture a precisely known volume of water. Furthermore, these results validate the choice of using motorized ball valves on either end of the PVC columns to capture the sample.

Preliminary Sediment Testing

Table 5.2 shows the mass added to the sample column as well as the measured pressure values for each sediment concentration from the preliminary sediment testing. Comparing the actual mass added to the mass calculated from each pressure reading provides a way to determine the accuracy at which the system measures. Table 5.3 presents the average error between the actual mass added and the calculated measured mass for the three replicates done at each concentration. The measured mass is calculated from the measured differential pressure reading. An added sediment density of 2.65 g cm^{-3} is assumed to perform this calculation. Initially, the accuracy goal of the design was to determine sediment mass for each concentration to within ±5%. However, after considering what the 5% corresponds to in terms of mass, evaluating the low concentrations based on measuring to 5% is unrealistic. For example, at 1000 mg L^{-1}, 5% of 0.5 g is 25 mg, which is the equivalent of 1 grain of 2mm sand. Realizing that measuring to the accuracy of being able to count sand grains is impractical, the goal for the minimum allowable error changed to the greater of 5% or 0.25 g (equivalent to about 500 mg L^{-1}), which is within the resolution that the Honeywell pressure transducer can measure. Testing verified that resolution as 0.25 g corresponds to 0.2% of the full-scale range, with the sensor rated at an accuracy of 0.1%. This changed the goal for the design to evaluate the pressure measurements across the various concentrations based on a target accuracy of the greater of 0.25 g or 5%. Table 5.3 also presents a comparison of the allowable percent error and the measured average absolute percent error based on the new accuracy goal.

As seen in Table 5.3, the system met the target accuracy for the 1,000 mg L^{-1}, 80,000 mg L^{-1}, and 100,000 mg L^{-1} concentrations. However, it did not meet the goal across the middle concentrations. Further analysis of the data indicates potential systematic error affecting the preliminary sediment testing. These tests used a 1/16-inch brass nipple to connect the 1/16-inch Cole Parmer tubing from the respective pressure transducer ports to the reference and sample cylinders. As mentioned in the Instrumentation section of Chapter Three, meniscal forces caused by the surface tension of the water inside the barbs/tubing greatly affect the pressure reading. Increasing the diameter of the tubing where the meniscus forms decreases the force of the meniscus and thus decreases the effect it has on the pressure readings. As discussed inAppendix F, changing the diameter of the barbs and the tubing from 1.6 mm (1/16 in.) to 6.4 mm (¼ in.)

Table 5.1. Results of volume repeatability tests with the valve-column design.

Replicates		**Water (g)**	
Test 1		525.42	
Test 2		525.68	
Test 3		525.38	
Test 4		525.48	
Test 5		525.37	
Test 6		525.55	
Test 7		525.50	
Test 8		525.54	
Test 9		525.62	
Test 10		525.68	
Average	525.52	Standard Deviation	0.10 g = 0.02%

Table 5.2. Sediment mass added to the sample column at each concentration and soil type for the preliminary sediment testing. The table also presents the theoretical pressure reading (in. of H_2O) and the pressure reading (in. of H_2O) measured by the Honeywell RSC differential pressure transducer.

Soil Type	Concentration	Mass Added (g)	Theoretical Pressure Reading (in. of H_2O)	Measured Pressure Reading (in. of H_2O)
Sand	1,000	0.5	0.024	0.041
Sand	1,000	0.49	0.023	0.034
Sand	1,000	0.49	0.023	0.032
Silt	4,000	1.96	0.094	0.161
Silt	4,000	1.96	0.094	0.165
Silt	4,000	1.96	0.094	0.146
Clay	4,000	1.98	0.094	0.178
Clay	4,000	1.96	0.094	0.153
Clay	4,000	1.96	0.094	0.157
Sand	10,000	4.92	0.235	0.282
Sand	10,000	4.92	0.235	0.255
Sand	10,000	4.92	0.235	0.239
Sand	50,000	24.53	1.170	1.052
Sand	50,000	24.53	1.170	1.002
Sand	50,000	24.53	1.170	1.023
Sand	80,000	39.2	1.870	1.937
Sand	80,000	39.2	1.870	1.842
Sand	80,000	39.2	1.870	1.830
Silt	80,000	39.12	1.867	2.005
Silt	80,000	39.12	1.867	2.011
Silt	80,000	39.12	1.867	2.023
Clay	80,000	39.24	1.872	1.862
Clay	80,000	39.24	1.872	1.869
Clay	80,000	39.24	1.872	1.865
Sand	100,000	49.05	2.340	2.160
Sand	100,000	49.05	2.340	2.230
Sand	100,000	49.05	2.340	2.263

Table 5.3. Comparison between the average absolute error and the allowable percent error based on the refined accuracy goal of the greater of 0.25 g or 5%. For the concentrations at which multiple sediment types were run (4000 and 80000 mg L^{-1}), the results represent the average of all replicates over all sediment types. The other concentrations were just run for three sand replicates.

Preliminary Sediment Tests			
Soil Type	Target Concentration (mg L^{-1})	Average Absolute % Error	Allowable % Error
Sand	1,000	51.2	50
Silt	4,000	68.2	12.5
Clay	4,000	73.5	12.5
Sand	10,000	10.2	5
Sand	50,000	12.4	5
Sand	80,000	2.4	5
Silt	80,000	7.9	5
Clay	80,000	0.4	5
Sand	100,000	5.2	5

decreases the maximum potential error in the pressure reading from ±0.5 inches of water to ±0.08 inches of water. Although the error between tests can be less than these maximum values, it is clear that the dynamics of the meniscus forming in the 1.6 mm (1/16 in.) ports/tubing added error to the preliminary sediment testing results. Therefore, the system design used in the final sediment testing implemented this modification.

Additionally, data evaluation for the preliminary sediment test replicates indicated that such evaluation could not easily be automated. The variance in the meniscal forces seen by the pressure transducer also prevents automated establishment of a zero-pressure value, which corresponds to the pressure reading measured by the Honeywell transducer when both the reference and sample columns are full of clean water. If the height of the water column is equal in both cylinders, then the sensor should read a pressure differential equal to zero. Adding sediment to the sample column changes the differential pressure reading based on the added mass. Having a true zero-pressure value allows use of the maximum pressure reading measured after the cylinder unit inverts as the actual differential pressure caused by the suspended sediment. However, the establishment of a zero-pressure value was seen in the preliminary tests as not repeatable because of the randomness in the meniscus formation. Data evaluation for the preliminary tests was done by hand, examining the resulting curve to attempt to establish the zero value after settling.

Additionally, the opening of the Vent valve and the Drain valve at the start of sampling was seen to cause noise in the pressure signal both due to physical vibrations and to a meniscus forming across the ball valve opening. Once the ball valve opens more than 0.95 cm (1/2 in.), the meniscus breaks and each cylinder vents to the atmosphere. Because the time to completely open each valve is approximately 10 s, the time at which the meniscus breaks is on the order of several seconds. Consequently, the pressure readings captured during this time contain noise. Moreover, it is during this time that all the sediment is in suspension and the pressure measurement

accurately represents the sample. Plotting the measured pressure readings versus the sampling time allowed for a manual method of visually analyzing the data to determine what the true maximum pressure value is. This violates the requirement of autonomous operation.

Final Sediment Testing

A series of six clean water tests prior to the final sediment testing showed that the larger 6.35 mm (¼ in) adapter and tubing leading from the cylinders to the pressure transduced allowed for somewhat more repeatable zero pressure values. Figure 5.1 shows the measured concentration (mg L^{-1}) versus time plot of the six clean water tests. The figure shows that by the end of the sampling period, the concentration for each test approaches a constant zero pressure value, but that these zero-pressure value vary by up to 4,000 mg L^{-1} in spite of the improved behavior using the larger adapter and tubing between the cylinders and the transducer.

To obtain a baseline raw pressure value used for evaluating each final sediment test, the raw pressure value is averaged across the six tests. Averaging these tests showed that the raw pressure reading corresponding to the system's zero pressure value is 15,456,000. Figure 5.2 shows the measured concentration (mg L^{-1}) versus time plot of the averaged six clean water tests. After 5 s of collecting data, the measured concentration (mg L^{-1}) stabilizes at zero, corresponding to a raw differential pressure value of 15,456,000. Furthermore, this testing shows that during the first 5 s of sampling, the meniscus formed across the Vent and Fill valves greatly affects the pressure

Looking at Figure 5.3, there is a repeatable trend in the pressure signal prior to the meniscus breaking. At first, the meniscus forms across a small diameter (corresponding to the valve just beginning to open), exerting a larger force. Both Figure 5.1 and Figure 5.2 convey this relationship as the raw pressure reading is highest at the beginning of the 5 s interval. As the valve opens and the meniscus force decreases, the raw pressure reading decreases. Once the meniscus breaks, a small shockwave travels through the column of water until the signal levels off at the true zero-pressure value. Because the initial trend is repeatable across all six water tests, fitting a polynomial to the first 5 s of the recorded data provides a compensation method for the meniscus effect. In theory, fitting a polynomial equation to the first 5 s of the data removes the offset caused by the meniscus and brings the pressure readings to the true zero-pressure value. Figure 5.3 shows the polynomial used to counteract the offset in the differential pressure. Use of the polynomial allows for removal of this initial valve meniscus effect, proving a better initial maximum pressure value.

With the zero-pressure value established by the clean water tests, the next step is to conduct the final sediment testing. Table 5.4 shows the mass added to the sample column for each concentration and soil type. It also presents the maximum measured pressure after adjustment for each replicate. The method for obtaining the pressure shown is as follows. First, the polynomial equation shown in Table 5.5 was used to subtract the zero-pressure valve meniscus value from the raw differential pressure measured by the Honeywell pressure transducer, resulting in a raw differential pressure caused solely by the addition of sediment mass to the sample cylinder. The resulting maximum raw differential pressure corresponds to the time at which all the sediment is in suspension. The next step is to add this max raw differential pressure value to the averaged raw zero-pressure value obtained during preliminary zero-

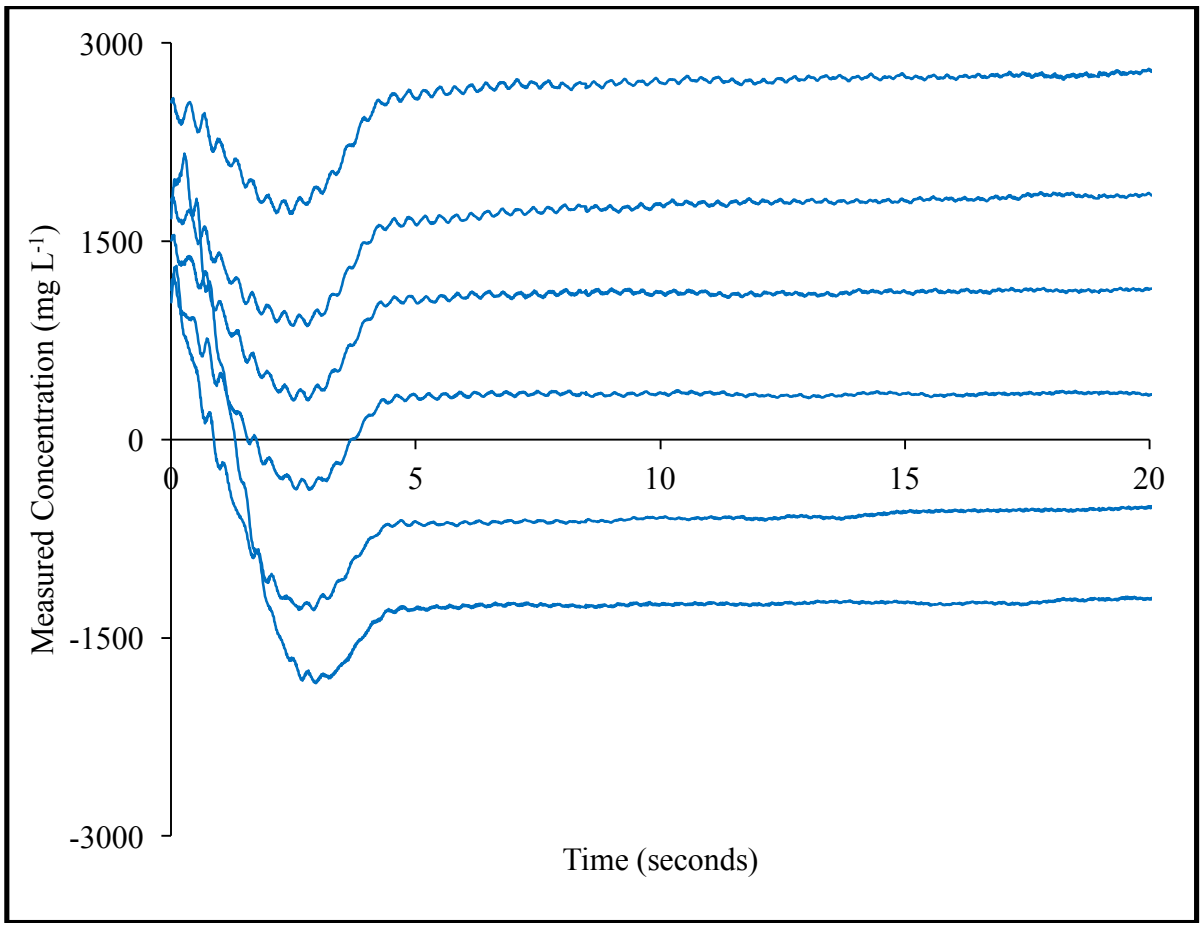

Figure 5.1. Plot showing the measured concentration (mg L^{-1}) for the six clean water tests. After the first 5 s, the pressure reading becomes constant at that test's zero-pressure value. The dips during the first 5 s indicate the impact of the valve meniscus formation, while the range of subsequent in steady-state values is indication of continued variability in zero-pressure values in spite of the larger adapter and tubing. The maximum variation between the six clean water tests is 4,000 mg L^{-1}.

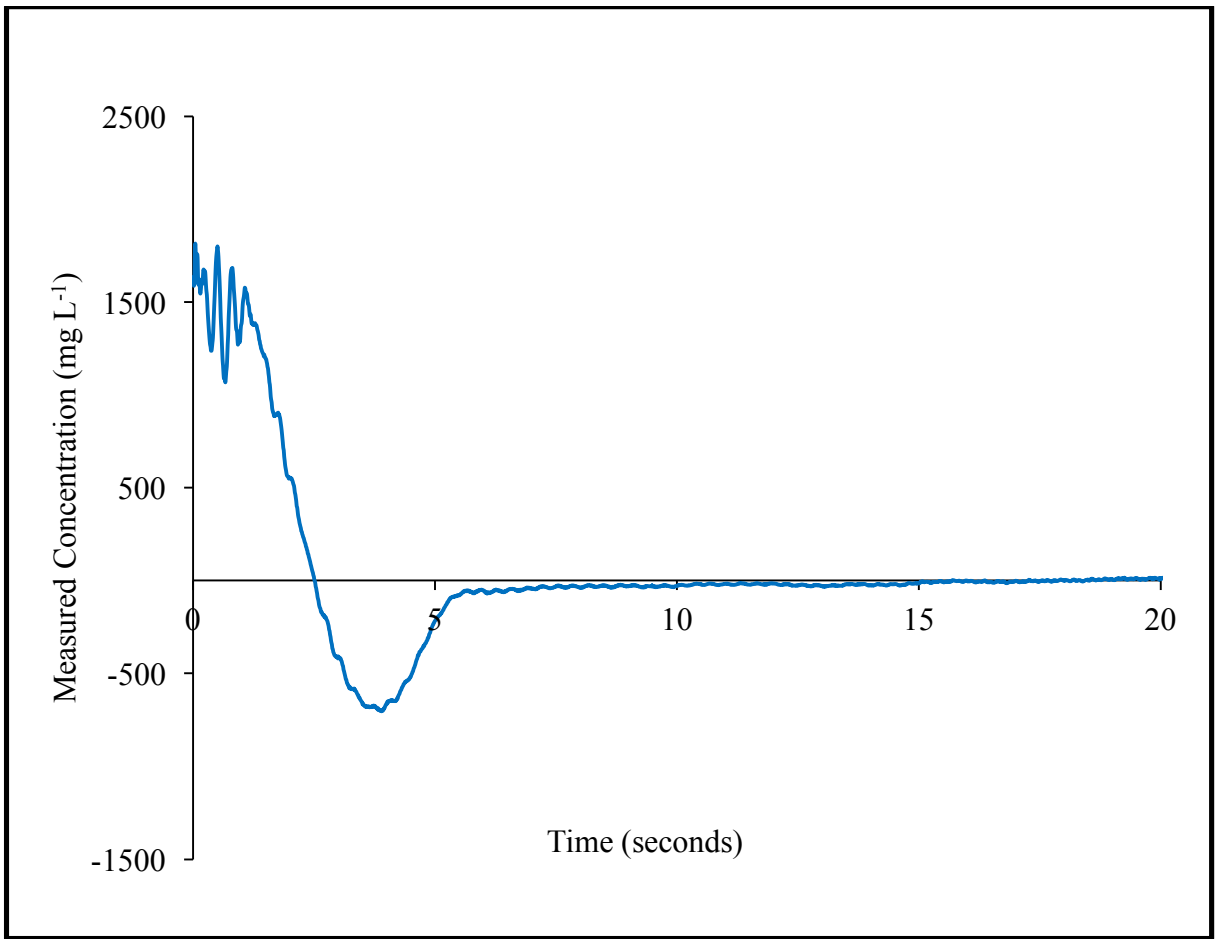

Figure 5.2. Plot showing the averaged measured sediment concentration (mg L^{-1}) for the six clean water tests. The plotted concentration values are obtained by averaging each test's corresponding concentration value, across all six tests. After the first 5 s, the measured signal becomes constant at a concentration of approximately zero.

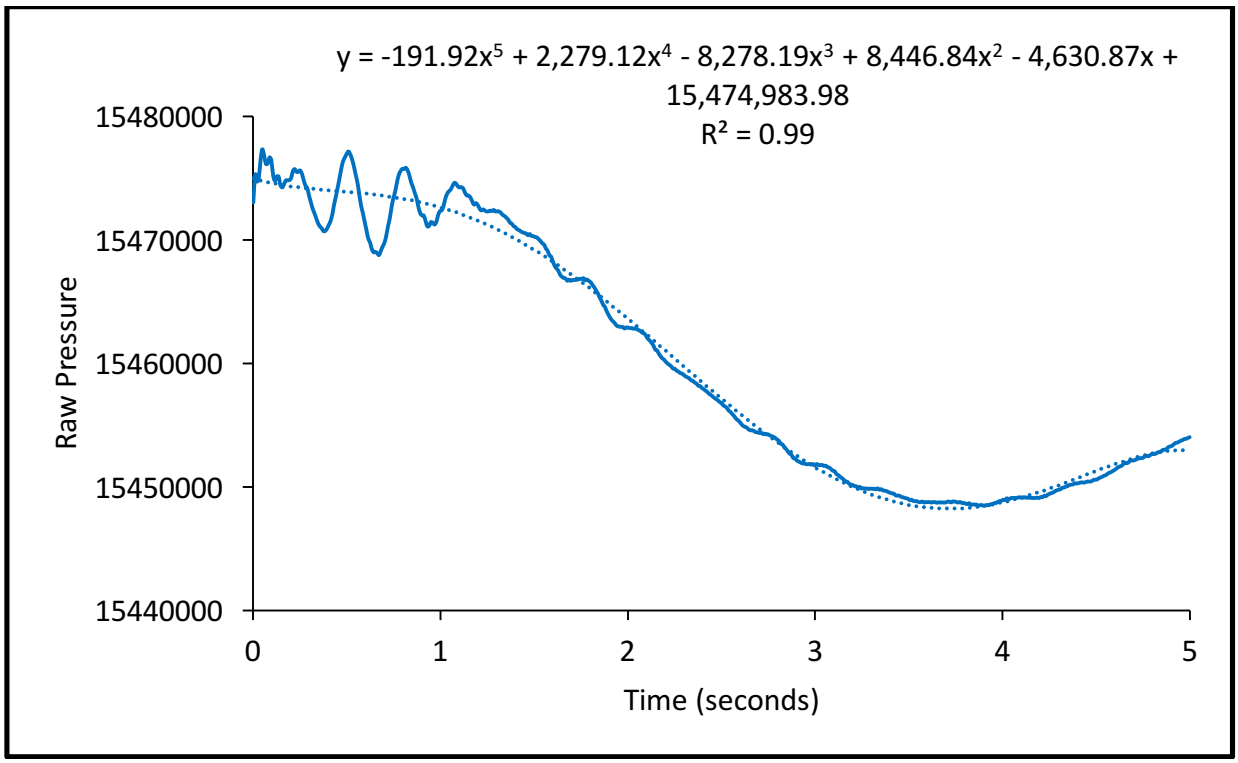

Figure 5.3. Plot showing the averaged raw pressure values for the six clean water tests and the best-fit polynomial over the first 5 s of data collection. This shape is consistent across all six individual tests. The figure also contains the associated polynomial equation and R^2 value.

Table 5.4. Mass added to the sample column in final sediment testing at each concentration and soil type, and the maximum adjusted pressure reading (in. of H_2O) measured by the Honeywell RSC differential pressure transducer.

Soil Type	Concentration	Mass Added (g)	Theoretical Pressure Reading (in. of H_2O)	Measured Pressure Reading (in. of H_2O)
Sand	500	0.26	0.012	0.128
Sand	500	0.26	0.012	0.078
Sand	500	0.26	0.012	0.153
Sand	1,200	0.59	0.028	0.115
Sand	1,200	0.57	0.027	0.264
Sand	1,200	0.58	0.028	0.267
Silt	1,200	0.51	0.024	0.207
Silt	1,200	0.46	0.022	0.242
Silt	1,200	0.49	0.023	0.246
Clay	1,200	0.53	0.025	0.176
Clay	1,200	0.49	0.023	0.141
Clay	1,200	0.42	0.020	0.135
Sand	12,000	5.84	0.279	0.344
Sand	12,000	5.85	0.279	0.391
Sand	12,000	5.89	0.281	0.367
Silt	12,000	5.65	0.270	0.156
Silt	12,000	5.77	0.275	0.236
Silt	12,000	5.64	0.269	0.428
Clay	12,000	5.61	0.268	0.228
Clay	12,000	5.81	0.277	0.243
Clay	12,000	5.63	0.269	0.272
Sand	120,000	58.76	2.804	2.637
Sand	120,000	58.73	2.802	2.421
Sand	120,000	58.91	2.811	2.803
Silt	120,000	58.74	2.803	2.171
Silt	120,000	58.74	2.803	2.140
Silt	120,000	58.71	2.801	2.171
Clay	120,000	58.79	2.805	2.765
Clay	120,000	58.75	2.803	2.809
Clay	120,000	58.75	2.803	2.791

Table 5.5. Zero-pressure values used for each of the final sediment testing concentrations. Additionally, the table shows the polynomial equation fit to the first 5 s of each clean water test. As one can see, the zero-pressure value increases over the course of the testing due to sediment accumulation in the port.

Concentration	Raw Zero-Pressure	Polynomial Equation
1,200 mg L^{-1}	15,456,000	$y = -192x^5 + 2{,}279x^4 - 8{,}278x^3 + 8{,}447x^2 - 4{,}631x + 15{,}474{,}984$
12,000 mg L^{-1}	15,545,300	$y = -48x^6 + 1{,}082x^5 - 9{,}439x^4 + 38{,}726x^3 - 69{,}169x^2 + 16{,}255x + 15{,}602{,}950$
120,000 mg L^{-1}	15,701,300	$y = -7x^6 + 154x^5 - 1{,}420x^4 + 7{,}106x^3 - 16{,}872x^2 + 949.22x + 15{,}746{,}903$

pressure testing, which was 16,287,382 (see Appendix I). A final empirical equation shown in Appendix I relates this raw differential pressure to a measured differential pressure in depth of water, as presented in Table 5.4.

It was also observed during the final sediment testing that some sediment added to the sample cylinder collected in the 6.35 mm (¼ in.) adapter port in the sample cylinder, so some small part of the added sediment was not suspended in the column after flipping. Additionally, as testing continued, the sediment deposited in the port was not removed by the natural flushing of the sample cylinder. Sediment in the port effectively decreased the port size, affecting the formation of the meniscus and thus the differential pressure measurements. Clean water tests run after the 12,000 mg L^{-1} and 120,000 mg L^{-1} sediment replicates demonstrated the effect of this error. Upon evaluation of these tests, it was evident that the zero-pressure value of the system changed over the course of the testing due to this effect. Table 5.5 shows the zero-pressure shift over time, with the zero-pressure value increasing over the final sediment tests. Furthermore, the clean water tests at 12,000 mg L^{-1} and 120,000 mg L^{-1} exhibit the same valve-meniscus behavior during the first 5 s of sampling seen in the initial clean water tests. Table 5.5 also shows the polynomial equation fit to the first 5 s for the three different clean water tests. The differential pressure calculations presented in Table 5.4 come from these three compensation equations. Furthermore, Table 5.6 presents a comparison of the allowable percent error and the average absolute percent error based on the accuracy goals established in the preliminary sediment testing. The error presented is calculated based on the average error between the actual mass added and the calculated measured mass for the three replicates done at each concentration. The measured mass is calculated from the measured differential pressure reading shown in Table 5.4

As seen in Table 5.6, the autonomous system was only able to meet the accuracy goals for the clay test at 120,000 mg L^{-1}. However, the error decreases as the sediment concentration increases. One explanation for this is that sediment accumulating in the adapter port (and thus not suspended in the sample cylinder after rotation) has a greater impact on the lower concentrations. For example, 0.25 g of sediment accumulating in the port corresponds to almost 50% of the total detectable mass at 1,200 mg L^{-1}, whereas 0.25 g of sediment at 120,000 mg L^{-1} corresponds to only 0.4% of the total detectable mass. Thus, a small mass of sediment deposited in the port will increase the error in the measured differential pressure more for the low

Table 5.6. Comparison between the average absolute error and the allowable percent error based on the refined accuracy goal of the greater of 0.25 g or 5%.

Final Sediment Tests			
Soil Type	Target Concentration (mg L^{-1})	Average Absolute % Error	Average Allowable % Error
Sand	1,200	681.4	42.4
Silt	1,200	900.9	42.4
Clay	1,200	557.4	42.4
Sand	12,000	31.4	5
Silt	12,000	38.5	5
Clay	12,000	9.4	5
Sand	120,000	6.6	5
Silt	120,000	22.9	5
Clay	120,000	0.7	5

concentrations. Also, as discussed previously, sediment depositing in the tubes increases the force of the meniscus forming across the port and affected the zero-pressure reading, which once again has a larger impact on the measured error at the lower concentrations.

Additionally, plotting the measured concentration (mg L^{-1}) versus sampling time for each of the test replicates indicates that applying the polynomial equations over the first 5 s of the test does not fully compensate for the effect of the meniscus across the opening valves. As Figures 5.4, 5.5, and 5.6 show, the meniscus formation over the initial 5 s of sampling has a more significant impact on the signal at the lower concentrations because it represents a higher percentage of the total signal measured. These figures represent clay, silt, and sand tests at 1,200 mg L^{-1}, 12,000 mg L^{-1}, and 120,000 mg L^{-1} respectively. It should be noted that the soil type used in Figures 5.4, 5.5, and 5.6 does not affect the signal shape over the first 5 s of sampling. The electronic files provided to the committee members contain the raw pressure versus time plots for each soil type and concentration for each replicate. Furthermore, the technique of using the maximum raw differential pressure to determine mass added is greatly affected by the valve meniscus effect. The lower the concentration, the more effect the meniscus has on the measured differential pressure, and thus the more variance in the maximum differential pressure recorded. The minimum raw signal that the system needs to detect is roughly 3500 data counts, corresponding to 0.25g or 500 mg L^{-1}. Analyzing the data shows that the variance in the signal due to valve meniscus formation is 20 times greater than this, while variance in the signal due to the system's inability to establish and maintain a zero-pressure is on the order of 60 times larger than 3500 counts. In addition to that, Figures 5.4, 5.5, and 5.6 show that the zero-pressure value changed over the course of testing due to sediment deposition in the adapter.

Operational Testing

Individual testing of each system component was successful, allowing the entire system to be tested as an assembled autonomous device. With the pumps providing a continuous supply of clean water, the system operated as designed for multiple cycles, indicating it could function

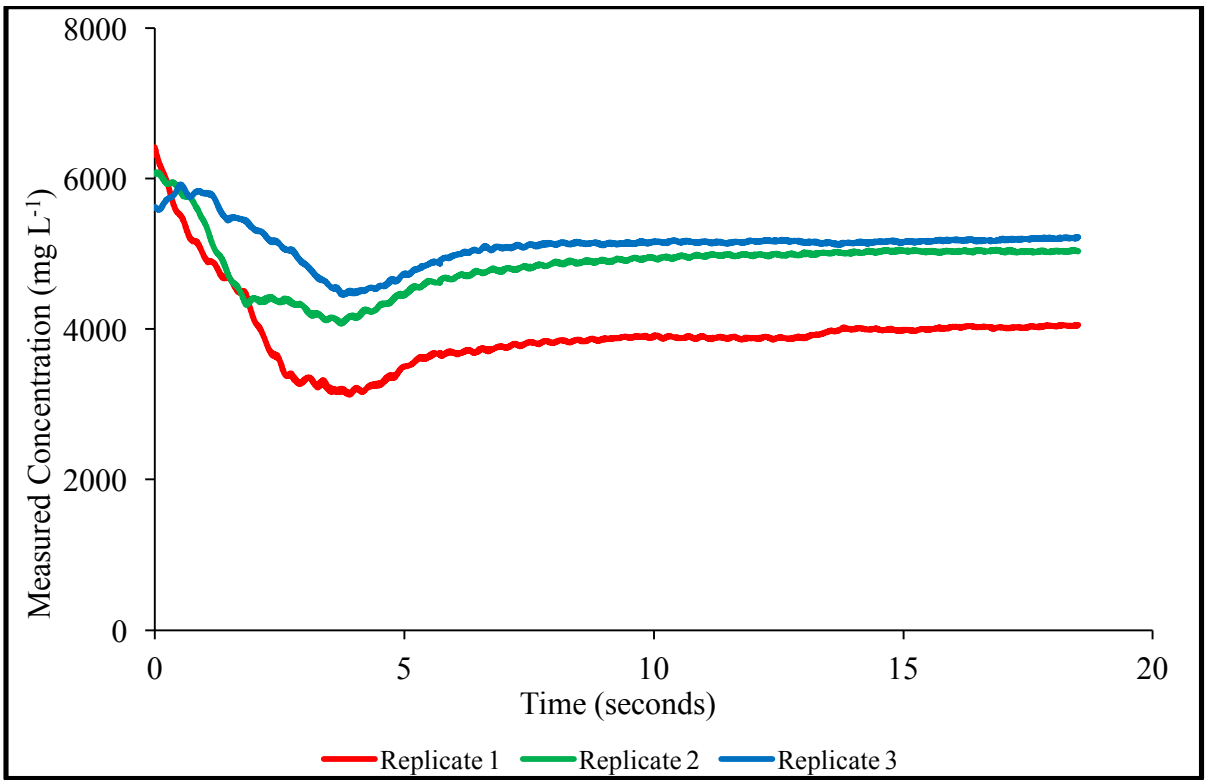

Figure 5.4. Measured sediment concentration (mg L^{-1}) over time for the clay tests done at 1,200 mg L^{-1}. The plot contains each of the three replicates done at that concentration and soil type. The effect of the meniscus on the first 5 s of the signal is relatively repeatable, and is greatest at this low concentration.

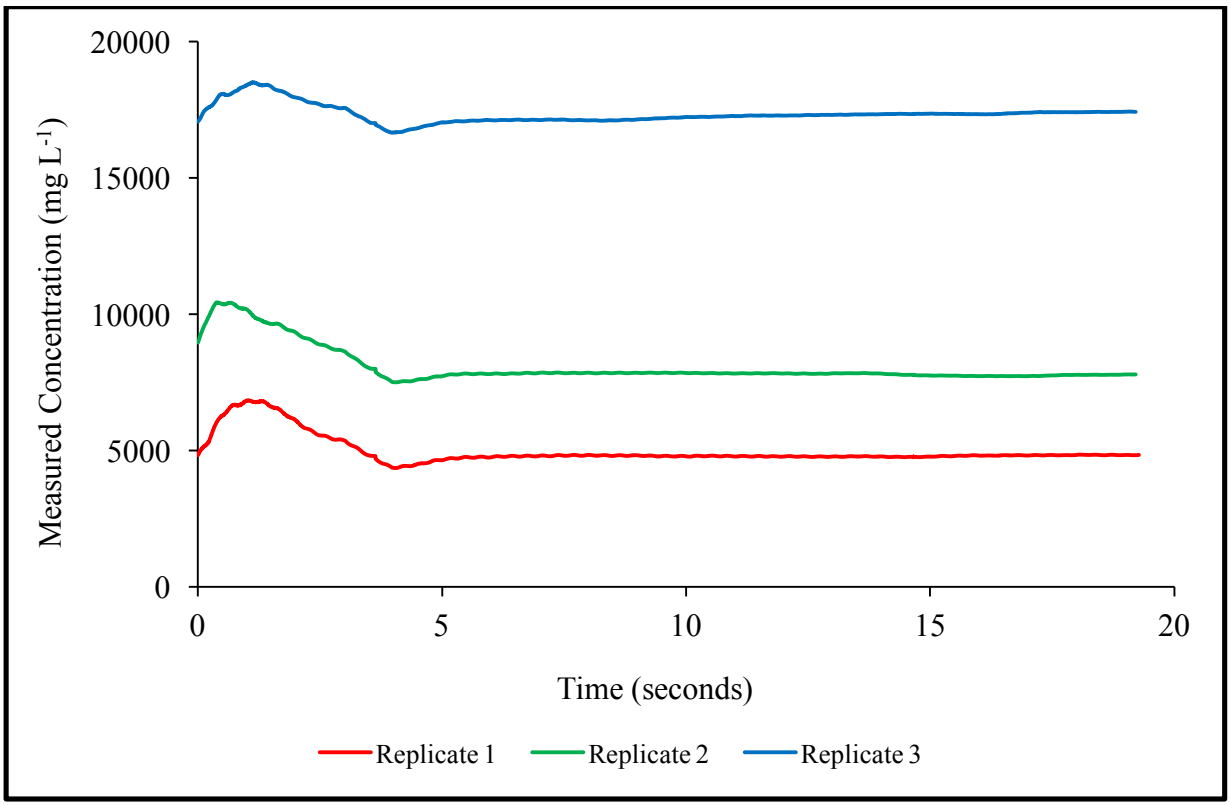

Figure 5.5. Measured sediment concentration (mg L^{-1}) over time for the silt tests done at 12,000 mg L^{-1}. The plot contains each of the three replicates done at that concentration and soil type. The effect of the meniscus on the first 5 s of the signal is evident but less significant than at the lower concentration of 1,200 mg L^{-1}.

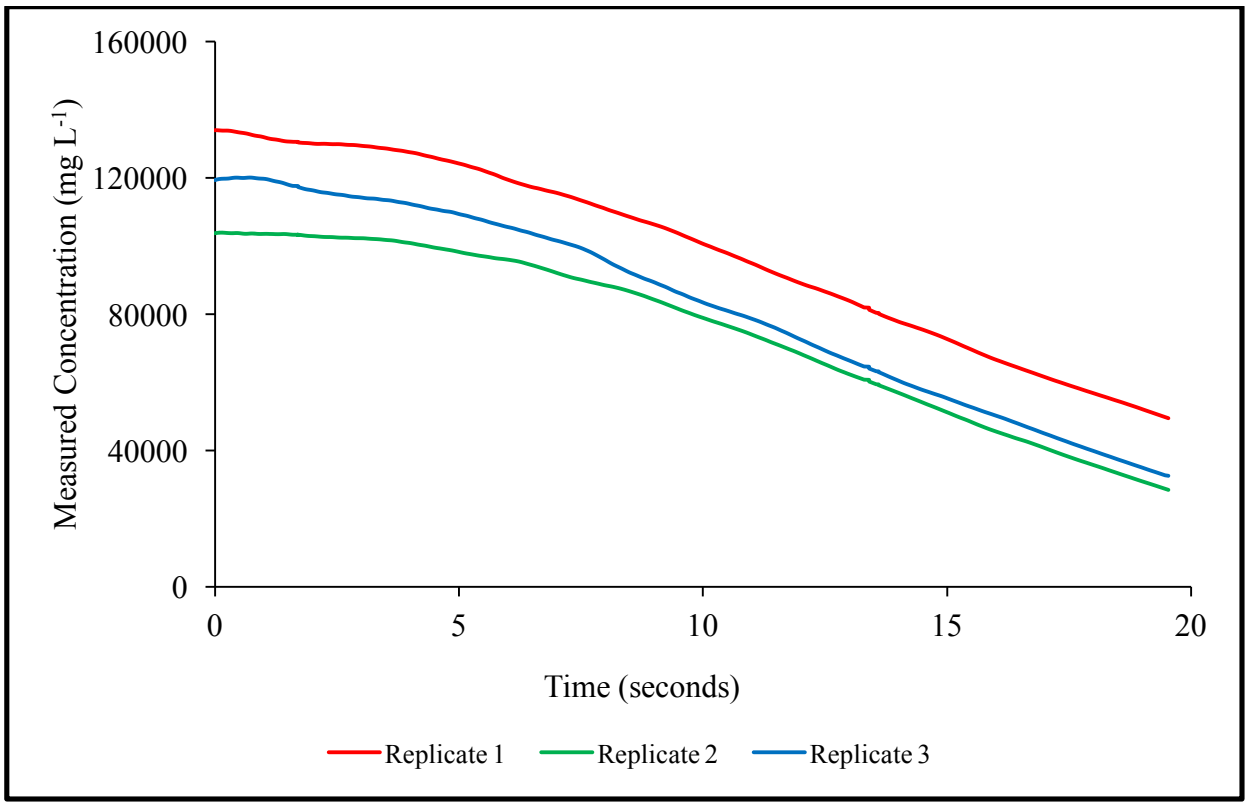

Figure 5.6. Measured sediment concentration (mg L^{-1}) over time for the sand tests done at 120,000 mg L^{-1}. The plot contains each of the three replicates done at that concentration and soil type. The effect of the meniscus on the first 5 s of the signal is barely visible as a small blip, much less significant than at the lower concentrations.

without human interaction.

It should be noted that the stainless steel axle used to support and rotate the cylinder unit did show visual signs of bending. Although this did not affect the motor's ability to rotate the cylinder unit, it did cause a slight oscillation in the axle during rotation.

Environmental Chamber Testing

Comparing the sediment mass results for the temperature tests run at 5°C, 20°C, and 40°C is not of much value, based on the results of the final sediment testing. The inability to establish and maintain a zero-pressure value and the impact of the valve meniscus formation meant that analyzing the effect of temperature on the design's ability to detect sediment mass is unfeasible. Therefore, comparing the test data collected for the hot, cold, and room temperature tests at 12,000 mg L^{-1} is more qualitative, concentrating on the questions related to system operation. Specifically, plotting the measured differential pressure versus sampling time provides insight into the fall velocity of the sand with respect to water viscosity. Table 5.7 shows the change in water viscosity due to temperature as found in Sturm (2001). Figure 5.7 represents the measured sediment concentration (mg L^{-1}) versus time for each of the temperature tests at 12,000 mg L^{-1}. The figure indicates that the fall velocity increases with temperature, as predicted by Stokes Law (see Appendix J). At the end of the 20 s sampling time, both the hot and room temperature plots begin to level off, indicating that most if not all of the sand resides below the port. Conversely, the slope of the cold temperature plot suggests that there is still sand settling through the column at the end of the 20 s interval.

Another result from the environmental chamber testing is that the aluminum hubs attaching the cylinder unit to the stainless steel axle are sensitive to temperature change. The different thermal expansion coefficients of aluminum and steel caused loosening of the cylinder unit connection to the stainless steel axle when subjecting the design to a temperature of 5°C. This resulted in the flipping motor being unable to rotate the cylinder unit. Additionally, when the system was at 5°C the timing crystal on the HB-25 motor controller got out of sync with the timing crystal on the main Teensy 3.2. This was observed when the motor attempted to rotate the cylinder unit in the counter-clockwise direction even when the Teensy sent a pulse time of 1.5 ms, which should result in turning the motor off. Lack of synchronization between the two timing chips would change this pulse width, seen by the motor as a command to move. The HB-25 data sheet does not provide an operating temperature range, so it is possible that at the low temperature of 5°C the controller does not operate as designed. A small change in the timing between the two crystals can have a significant impact, especially when that small change is seen as the difference between an "on" or "off" state. However, further investigation into this occurrence is necessary to verify this interpretation.

Table 5.7. Theoretical differences in water dynamic viscosity at the tested temperatures, based on Sturm (2001).

Temperature (°C)	Dynamic Viscosity (N s/m^2)
5	1.519×10^{-3}
20	1.002×10^{-3}
40	0.653×10^{-3}

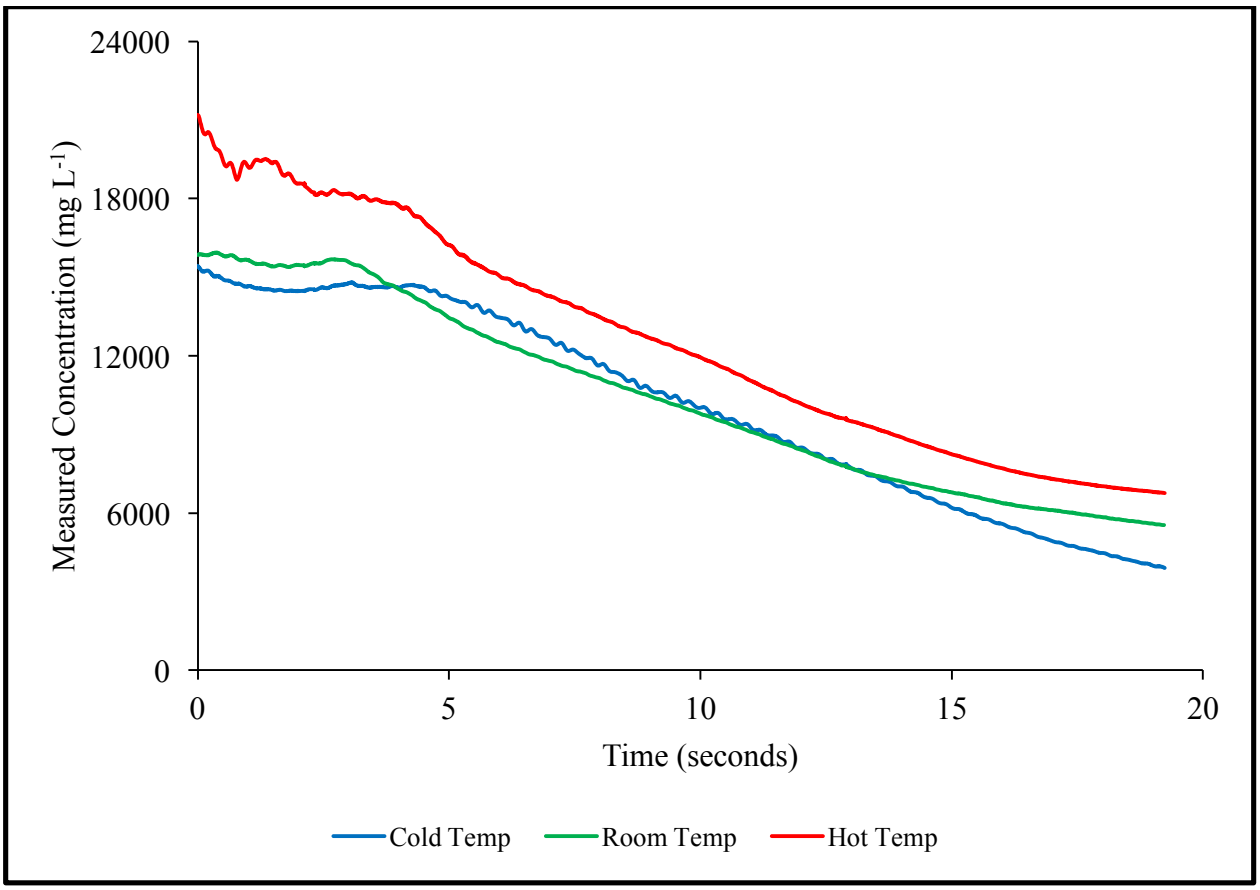

Figure 5.7. Measured sediment concentration (mg L^{-1}) over time for the sand test done at 12,000 mg L^{-1}. The plot contains each of the three replicates done at that concentration and soil type. The tests at the higher temperature show substantial leveling off of the signal near the end of the tests, indicating that the sand was already settled. The continued downward trend for the cold test indicate that the sand was still settling, likely due to greater water viscosity.

Robustness Testing

Final robustness and performance testing of the system showed that the 1" Deelat motorized ball valves used on the sample column fail over time when exposed to multiple cycles of sediment-water mixture. After 10 cycles (15 min) of recirculating 60,000 mg L^{-1} sediment-water, the Drain valve began leaking. The fine sand and silica particles in the water appeared to wedge between the stainless steel ball and the Nylon valve seat. Repeated opening and closing of the valve resulted in the entrapped particles scoring the Nylon, allowing water to leak through the valve.

However, prior to the Drain valve leaking, the system operated as intended. With power provided to the system, it autonomously sampled the recycled flow at a rate of a sample every 90 s. The main Teensy stored the measured differential pressure on the microSD in the form of non-volatile memory. Additionally, the XBee Pro on the main board read the stored pressure data from the microSD and wirelessly transmitted the data to a receiving XBee without any lost or fragmented data.

Table 5.8 presents the average RMS current draw across the three measured cycles for each stage in the sampling process. The time the system spends in each state is also shown, with the total cycle time equaling 90 s. As expected, the highest current draw occurs during rotation. Using these measured values, the total energy required to operate the system for three continuous days of sampling (based on a 90 s sampling period) is 57 A-hrs. This energy requirement is less than half the original theoretical maximum energy calculation of 120 A-hrs, which is reasonable because the initial calculation was based on each component's maximum current draw presented in the component's datasheet. Note that this energy consumption could be supplied by a normal deep-cycle 12V battery, and could be easily lengthened by adding additional energy sources (e.g., solar panels) to the system.

Table 5.8. Average RMS current (A) for each stage in the sampling cycle along with the time (s) the system operates in that state.

Cycle Stage	Average RMS Current (A)	Time (s)
Filling	0.9	5
Closing	0.8	15
Flipping	1.5	5
Reading	0.6	20
Closing	0.75	15
Flipping	1.65	5
Flushing	0.7	25

CHAPTER SIX
CONCLUSIONS AND RECOMMENDATIONS

This project developed a prototype system designed to provide an alternative method for measuring sediment mass in a water sample. Testing this design proved that the approach can capture a repeatable, known sample volume to within 0.02% or 200 mg L^{-1}. Preliminary testing with real soils demonstrated that the system can measure sediment mass across a concentration range from 1,200 mg L^{-1} to 120,000 mg L^{-1} to within an accuracy of the greater of 0.25 g or 5%. However, the analysis used to obtain these accuracies relies on the establishment of a repeatable zero-pressure value. Final sediment testing verified this and further supported the theory that menisci forming across the motorized ball valves as well as those in the pressure lines greatly affect the differential pressure measurements. As designed, the prototype system operates autonomously, capturing and analyzing a 0.5 L water sample once every 90 s. The system can store the measured sediment mass data in the form of non-volatile memory. Additionally, its ability to transmit the captured data wirelessly allows it the functionality of being implemented in a remote setting.

Before implementing this design in the field, it is necessary to conduct further system redesign and testing. Robustness testing showed that while the Deelat motorized ball valves capture the desired volume, they cannot be used long-term, as the grinding of the sediment on the valve seat creates leaks. Additionally, the 10 s open/close time of the valves is too long. Not only does this operation time cause system noise due to vibrations, but it also allows the meniscus forming across the opening valves to affect the pressure measurement for an excessively long period. Based on these findings, a second-generation design should investigate alternative valve designs. Appendix K discusses ideas for replacing the motorized ball valves.

Future design efforts also need to address the issue of how a meniscus forms in the adapter pressure ports and lines, as this is critical in establishing a zero-pressure value and thus an accurate sediment mass calculation. Even though changing from a 1.6 mm (1/16 in.) to a 6.4 mm (1/4 in.) adapter and line greatly reduced this effect it is still far too large, yielding noise on the order of 10 times the desired minimum signal. Ideas for dealing with this are also discussed in Appendix K.

Design changes to not allow sediment to enter the pressure ports should also be implemented to improve the repeatability of meniscus formation, again allowing for a more consistent zero-pressure value. Appendix K describes methods for addressing this issue. Establishing a more stable zero-pressure value and further minimizing the influence of the valve menisci will allow for more sediment testing over the concentration ranges. This could include acquiring more insight into the influence temperature has on the differential pressure transducer.

Although the selected system components allow the design to operate in an autonomous manner, a redesign could reduce the number of components required. Using a gear motor with an absolute encoder would eliminate the need for the magnetic latches and the photogate. Additionally, a larger flipping motor and axle would provide more rigid support to the cylinder unit and reduce system shaking during rotation. Choosing a single wireless transmission method would reduce the board space required on the main PCB. Furthermore, because the design will be implemented in the field, harvesting energy to recharge the deep cycle battery should be considered as a more efficient way to power the design.

As suggested, further optimization of the system is required for the design to be considered field ready. However, the current system has taken the first step in proving the validity of the approach and in providing an autonomous method for capturing sediment concentration in a water sample. In doing so, it has shown promise that a measurement-based standard could be implemented for sediment load regulation.

LIST OF REFERENCES

American Society for Testing and Materials (ASTM). (2013). Standard test methods for determining sediment concentration in water samples: D 3977-97, vol. 11.02, Water (II), 395-400.

Durner, W., S. C. Iden, and G. von Unold(2017), The integral suspension pressure method (ISP) for precise particle-size analysis by gravitational sedimentation, Water Resour. Res.,53,33–48, doi:10.1002/2016WR019830

Ehrhart, B.J., Shannon, R.D., & Jarrett, A.R. (2002). Effects of construction site sedimentation basins on receiving stream ecosystems. *Transactions of the ASAE*, 45(3), 675-680.

Hayes, S.A., R.A. McLaughlin, and D.L. Osmond. (2005). Polyacrylamide use for erosion and turbidity control on construction sites. Journal of Soil and Water Conservation 60(4):193-199.

Lewis. A. J. and Rasmussen. T. C. (1996). A new passive technique for the in-situ measurement of total suspended solids concentrations in surface water. Tech. Completion Rep. for Project No. i4-0S-00l'G-20J3 (07), U.S. Dept. of the Interior. U.S. Geol. Survey, Reston. Va.

MacCurdy, M. G. (2010). EPA Construction Stormwater Rule Takes Effect February 1, 2010. *Marten Law*. Retrieved from: http://www.martenlaw.com/newsletter/20100120-construction-stormwater-rule#_edn3.

MacCurdy, M. G. (2014). EPA Revises CWA Construction Stormwater Rule; Removes Controversial Numeric Turbidity Limits. *Marten Law*. Retrieved from: http://www.martenlaw.com/newsletter/20140319-epa-revises-cwa-stormwater-rule.

Sturm, T. W. (2001). *Open channel hydraulics*. Boston: McGraw-Hill.

USEPA (U.S. Environmental Protection Agency). (2009). Development Document for Final Effluent Guidelines and Standards for the Construction and Development Category. EPA-821-R-09-010. U.S. Environ. Protection Agency, Office of Water, Washington D.C.

Walling, D. E., & Horowitz, A. J. (2005). *Sediment budgets* (Vol. 291): Int. Assoc. of Hydrol. Sci.

APPENDIX

Appendix A: Moment of Inertia / Torque Calculations

The following calculations were used to determine the torque required to rotate the cylinder unit 180° in 4 s. This calculation was used in selecting the gear motor used in the design. For this calculation, the cylinder unit is treated as two solid cylinders.

Known Values:
- The mass of each cylinder is 8.5 kg (accounts for valve and water weight).
- The radius of each cylinder is 0.0129 m
- The length of each cylinder is 1.2192 m
- The distance from the axis of rotation to each cylinder's center of mass is 0.0320

Using the Parallel Axis Theorem, the mass moment of inertia for each cylinder is calculated as follows:

$$I = I_{cm} + md^2$$

where I is the mass moment of inertia (kg m^2), I_{cm} is the mass moment of inertia about the cylinder's center of mass (kg m^2), m is the cylinders mass (kg), and d is the distance from the center of mass to the axis of rotation.

$$I_{cm} = \frac{1}{12} m(3r^2 + l^2)$$

where m is mass (kg), r is the radius of each cylinder (m), and l is the length of each cylinder (m).

Using these two equations to calculate the mass moment of inertia for each cylinder yields:

$$I = \frac{1}{12} * (8.5\ kg) * (3 * (0.0129\ m)^2 + (1.2192\ m)^2) + (8.5\ kg) * (0.032\ m)^2$$

$$I = 1.062\ kg\ m^2$$

Because each cylinder is treated as identical, the total mass moment of inertia is 2.124 kg m^2.

The torque required to rotate the cylinder unit 180° is calculated using the following equation:

$$\mathrm{T} = I\alpha$$

where T is the torque (N m), I is the total mass moment of inertia (kg m^2), and α is the angular acceleration (rad s^{-2}).
Calculating the angular acceleration is based on a trapezoidal acceleration curve with the system accelerating from rest to maximum speed in 1 s, holding the maximum speed for 2 s, before

decelerating from maximum speed to rest in 1 s. First, the angular velocity is calculated via the following equation:

$$\omega = \frac{d}{t}$$

where ω is the angular velocity in (radians s^{-1}), d is the total distance traveled (radians), and t is the time of rotation (s).

$$\omega = \frac{\pi}{2\ s}$$

The 2 s time of rotation is obtained from the acceleration curve as follows:

$$d = \omega t_1 + 2\left(\frac{\omega}{2}\right) t_2$$

where d is the total distance traveled (radians), t_1 is the time spent at maximum speed, and t_2 is the time to accelerate/decelerate.

$$\pi = \omega(2\ s) + 2\left(\frac{\omega}{2}\right)(1\ s)$$

This yields an angular velocity of 1.047 rad s^{-1}. Knowing that the gear motor must accelerate the cylinder unit to maximum speed in 1 s, the angular acceleration is equal to 1.047 rad s^{-2}. Based on this, the torque required to rotate the cylinder unit is:

$$\mathrm{T} = (2.124\ kg\ m^2) * (1.047\frac{rad}{s^2})$$
$$\mathrm{T} = 2.243\ N\ m$$

Therefore, the required torque necessary to rotate the cylinder unit 180° in 4 s is 2.243 N m (19.85 in lbs). Based on the 32 rpm ActoRobotics HD Premium Planetary Gear datasheet, the selected motor can supply 21 N m (186 in lbs) of torque, which is more than enough to invert the cylinders.

Appendix B: Max Differential Pressure Calculations

The following calculations were used to determine the maximum differential pressure between the reference and sample cylinders, using a maximum concentration of 120,000 mg L^{-1}.

Known Values:
- The volume of the sample cylinder is 490 cm^3.
- The height of the column of water in the sample cylinder is 0.95 m
- The height of the column of water in the reference cylinder is 0.965 m
- The mass of the sediment is 59.9 g
- The mass of the water in the sample column is 467.4 g
- The density of water is assumed to be 1000 kg m^{-3}

The difference in pressure between the two columns is calculated based on the following equation:

$$\Delta P = P_{Sample} - P_{Reference}$$

$$\Delta P = \rho_S g h_S - \rho_R g h_R$$

where P is pressure (Pa), ρ is fluid density (g m^{-3}), g is the gravitational constant (m s^{-2}), and h is the column height (m).

Plugging in the respective values for the two cylinders:

$$P_{Sample} = \left(\frac{0.0599\ kg + 0.4674\ kg}{0.00049\ m^3}\right) * \left(9.81\frac{m}{s^2}\right) * (0.95\ m) = 10{,}028.92\ Pa$$

$$P_{Reference} = (1000\ kg/m^3) * \left(9.81\frac{m}{s^2}\right) * (0.965\ m) = 9{,}466.65\ Pa$$

$$\Delta P = 10{,}028.92\ Pa - 9{,}466.65\ Pa$$

$$\Delta P = 562.27\ Pa$$

Therefore, the maximum differential pressure between the sample cylinder and the reference cylinder due to a sediment concentration of 120,000 mg L^{-1} is 562.27 Pa (2.26 in H_2O).

Appendix C: System Logic Flow

STATE	MicroSwitch	Servo	Liquid-Level Sensor (LLS)	Fill Valve	Drain Valve	Reservoir Valves	Vent Valve	Motor/Encoder	Photogate	Differential Pressure Sensor	Thermistors	Microcontrollers	MicroSD	XBee	Decision Logic
Not Sampling: System Off	LOW	DISCH.	LOW	OPEN	OPEN	CLOSE	CLOSE	OFF	HIGH	OFF	OFF	SLEEP	OFF	SLEEP	No flow coming to system.
Flow Detected	HIGH	DISCH.	LOW	OPEN	OPEN	CLOSE	CLOSE	OFF	HIGH	OFF	OFF	ON	OFF	SLEEP	Microswitch becomes depressed.
Filling Sample Column	LOW	SAMPLE	LOW	OPEN	CLOSE	OPEN	CLOSE	OFF	HIGH	OFF	OFF	ON	OFF	SLEEP	Servo oriented above 3/4" PVC.
Sample Column Full	LOW	SAMPLE	HIGH	OPEN	CLOSE	OPEN	CLOSE	OFF	HIGH	OFF	OFF	ON	OFF	SLEEP	Water level at Liquid-Level Sensor (LLS).
Clockwise Rotation	HIGH	DISCH.	HIGH	CLOSE	CLOSE	CLOSE	CLOSE	ON +	LOW	OFF	OFF	ON	OFF	SLEEP	Gear Motor rotating clockwise.
Sampling	HIGH	DISCH.	LOW	CLOSE	OPEN	CLOSE	OPEN	OFF	LOW	ON	ON	ON	WRITE	SLEEP	System inverted. Sediment is re-suspended.
Counter-Clockwise Rotation	HIGH	DISCH.	LOW	CLOSE	OPEN	CLOSE	CLOSE	ON -	LOW	OFF	OFF	ON	OFF	SLEEP	Gear Motor rotating counter-clockwise.
Draining Sample Column	HIGH	DISCH.	LOW	OPEN	OPEN	CLOSE	CLOSE	OFF	HIGH	OFF	OFF	ON	OFF	SLEEP	Disc hole aligned with photogate.
Continue Sampling	HIGH	DISCH.	LOW	OPEN	OPEN	CLOSE	CLOSE	OFF	HIGH	OFF	OFF	ON	OFF	SLEEP	Microswitch remains depressed.
Transmit Data	LOW	DISCH.	LOW	OPEN	OPEN	CLOSE	CLOSE	OFF	HIGH	OFF	OFF	ON	READ	WRITE	Done Sampling. Time to transmit.
Enter Low-Power State	LOW	DISCH.	LOW	OPEN	OPEN	CLOSE	CLOSE	OFF	HIGH	OFF	OFF	SLEEP	OFF	SLEEP	Runoff event over.

Figure A.1. System logic flow between states. The label “DISCH.” represents the servo arm positioned over the microswitch and thus the discharge system while “SAMPLE” corresponds to the servo arm positioned over the ¾” schedule 40 PVC aligned above the Sample cylinder. The “SLEEP” state represents the device placed in a low-power state. The conditions required for the system to enter a state are provided under the “Decision Logic” heading.

Appendix D: Main Printed Circuit Board Schematic

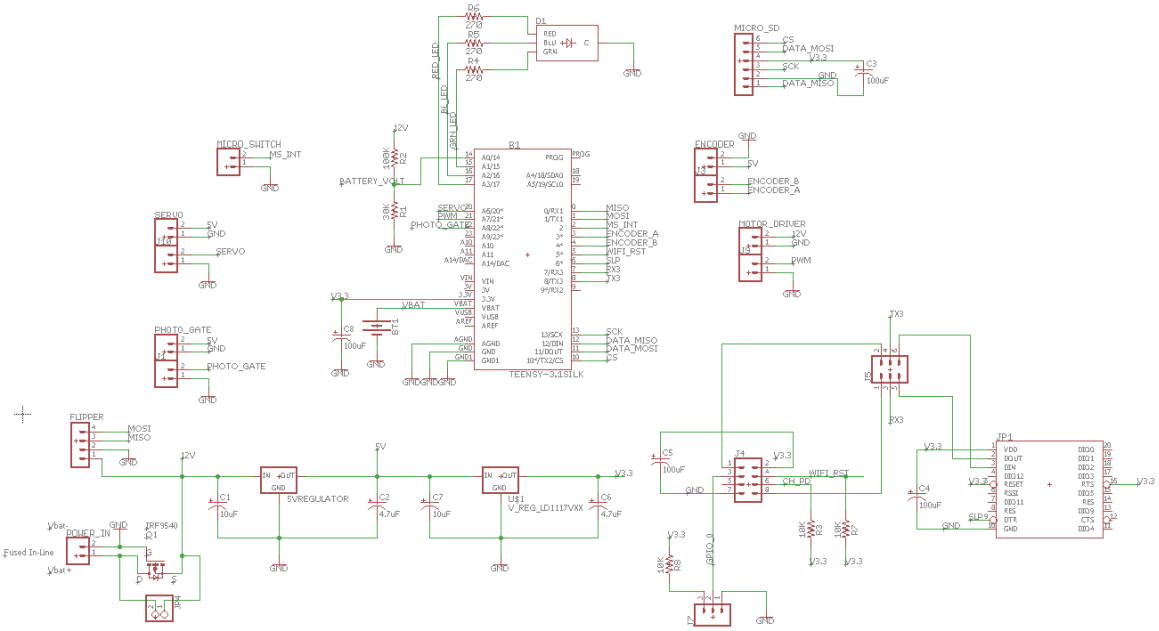

Figure A.2. The above image represents the schematic for the main printed circuit board.

Appendix E: Main Printed Circuit Board Layout

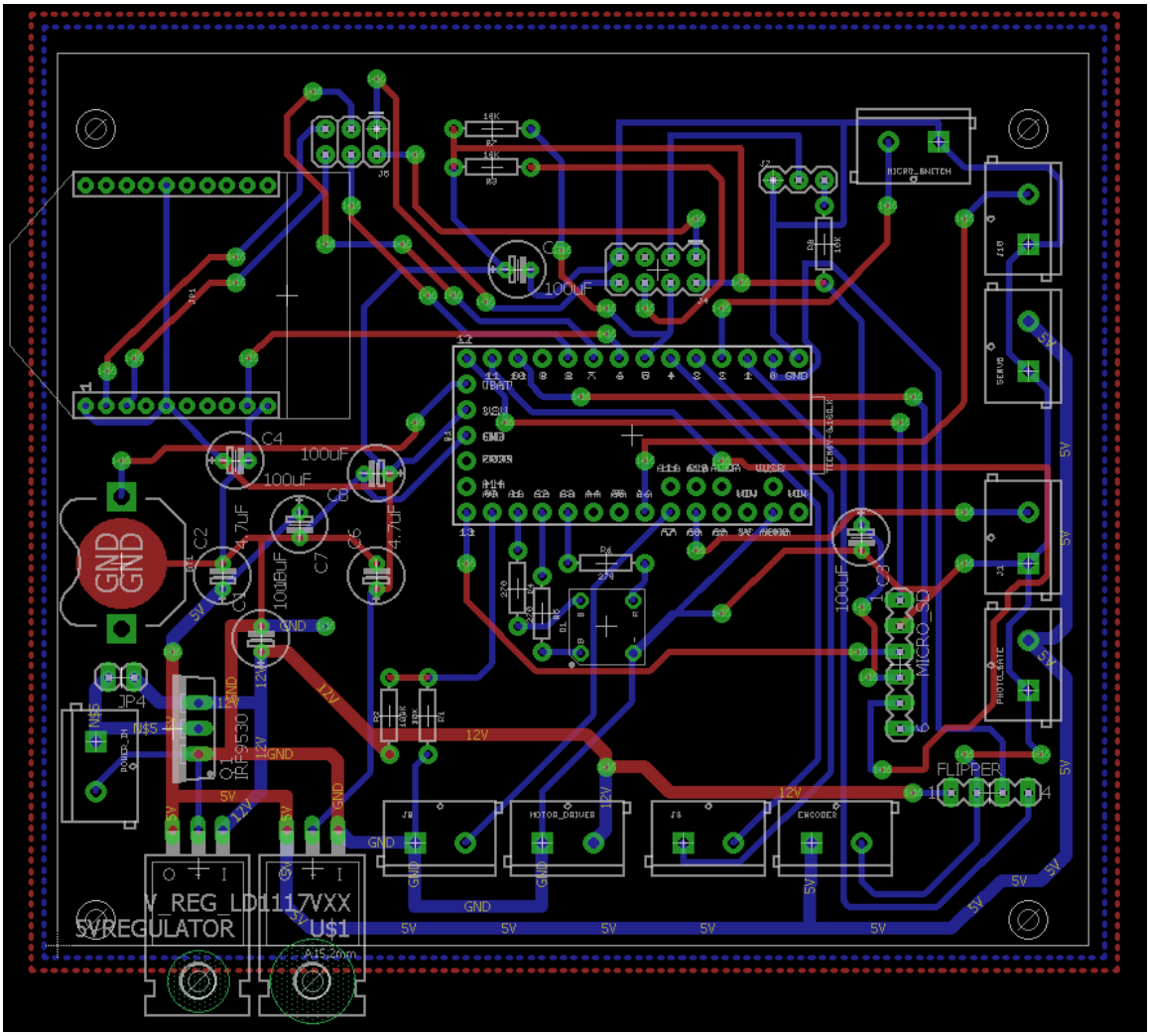

Figure A.3. The above image represents the board layout for the main printed circuit board.

Appendix F: Meniscus Testing

The theoretical height of a meniscus for water in a glass-tube at standard conditions is calculated using Jurin's Law:

$$H = \frac{0.0459}{d}$$

where H is the height of the meniscus (in. of water), d is the diameter of the tube (in.), and standard conditions consist of water on glass with an assumed wetting angle of 90° at 20ºC with a fluid density of 1000 kg/m^3 and a gravitational constant of 9.81 m/s^2.

A 1/16-inch barb diameter then corresponds to a calculated capillary rise of 0.73 inches of water. Using the Honeywell RSC differential pressure sensor, this rise corresponds to 36% of the 2-inch pressure reading. The unreliable raw pressure reading is not acceptable for the system; therefore, the effect of the meniscus needs to be minimized. To do this, the barb diameter must increase, which based on Jurin's law will decrease the capillary rise and hence decrease the force exerted by the meniscus. Based on this relationship, the 1/16-inch brass barb was initially replaced with a 1/8-inch barb. This decrease in diameter corresponded to a smaller raw pressure variance of +/- 50,000, and a calculated capillary rise of 0.37 inches, which represents 18% of the 2-inch pressure reading.

Jurin's law provides a means for theoretically calculating a barb diameter that creates the smallest force on the pressure sensor due to capillary rise. However, the relationship provided by Jurin's law is for water rising in a vertical column, yet the meniscus forming in this system is across a horizontal barb/tubing. Because the differential pressure sensor cannot be wetted, it is essential that a meniscus does form in the horizontal barb/tubing to prevent damage to the sensor. It is desired that the barb used in the system creates a meniscus with smallest capillary force. Therefore, simple lab tests showed that the largest diameter that a meniscus can form in horizontal tubing is ¼ inch. Based on these tests, a ¼ inch barb is used to translate the pressure from the column of water to the differential pressure sensor. The theoretical capillary rise calculated by Jurin's law for a ¼ inch diameter is 0.18 inches, or 9% of the 2-inch pressure reading. Furthermore, this increase in barb diameter resulted in a captured raw pressure variance of +/- 10,000. Although this increase in barb diameter to ¼ inch does not eliminate the effect of the meniscus on the pressure reading, it significantly minimized the error.

In addition to this issue, it is clear from testing that the meniscus effect is not repeatable. Repeatedly draining and filling the column resulted in a broad range of zero-pressure values. It appears that there is some randomness associated with the actual meniscus formation.

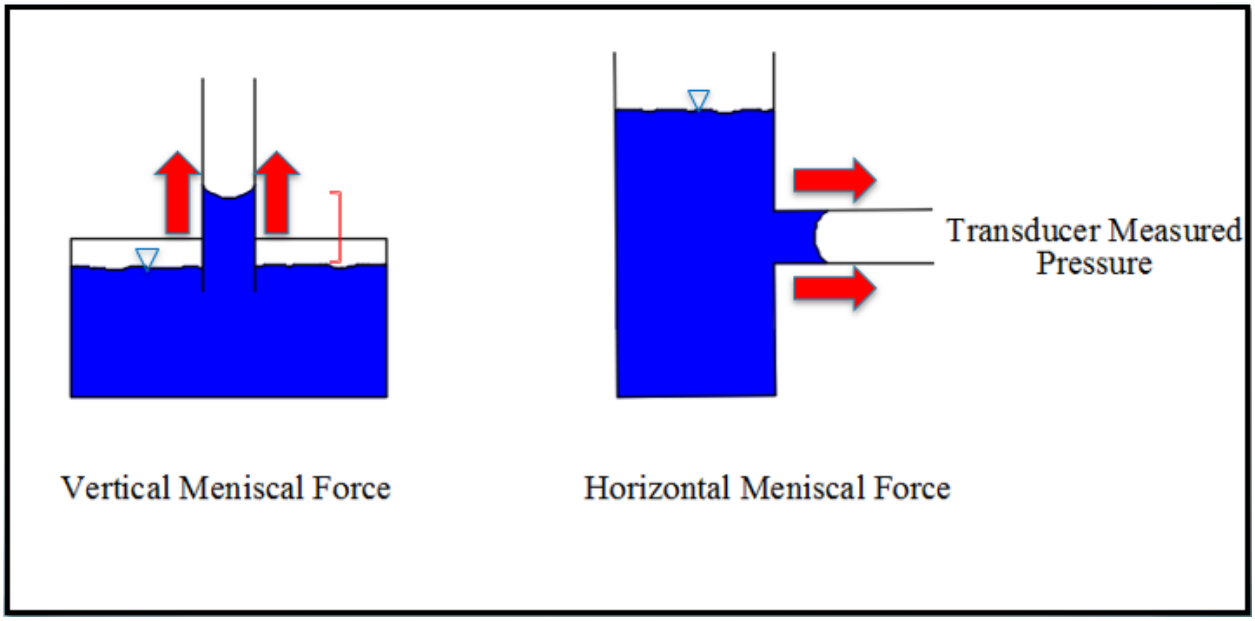

Figure A.4. Drawing of the meniscal forces acting in the vertical and horizontal planes. Typically, this force occurs in a vertical tube due to capillary rise. However, it acts in the horizontal plane for this system's design.

As shown in Figure A.3, the meniscal force acts along the perimeter of the tube and is caused by the adhesion forces of the water molecules to the tubing. The effect of the meniscal force is commonly seen in the case of capillary rise, which occurs in a vertical tube. The meniscal force is equal to the corresponding force due to gravity on the column of water in the tube. In the case of this design, the meniscal force acts in the horizontal plane. The pressure measured by the transducer equals the resulting pressure due to the height of the water column above center of the tube plus the meniscal force acting around the perimeter of the tube. Creating a contact angle of 90 degrees would result in the pressure seen on either side of the meniscus to be equal. This is the ideal scenario as it would eliminate the influence of the meniscus on the measured pressure.

Appendix G: Secondary Printed Circuit Board Schematic

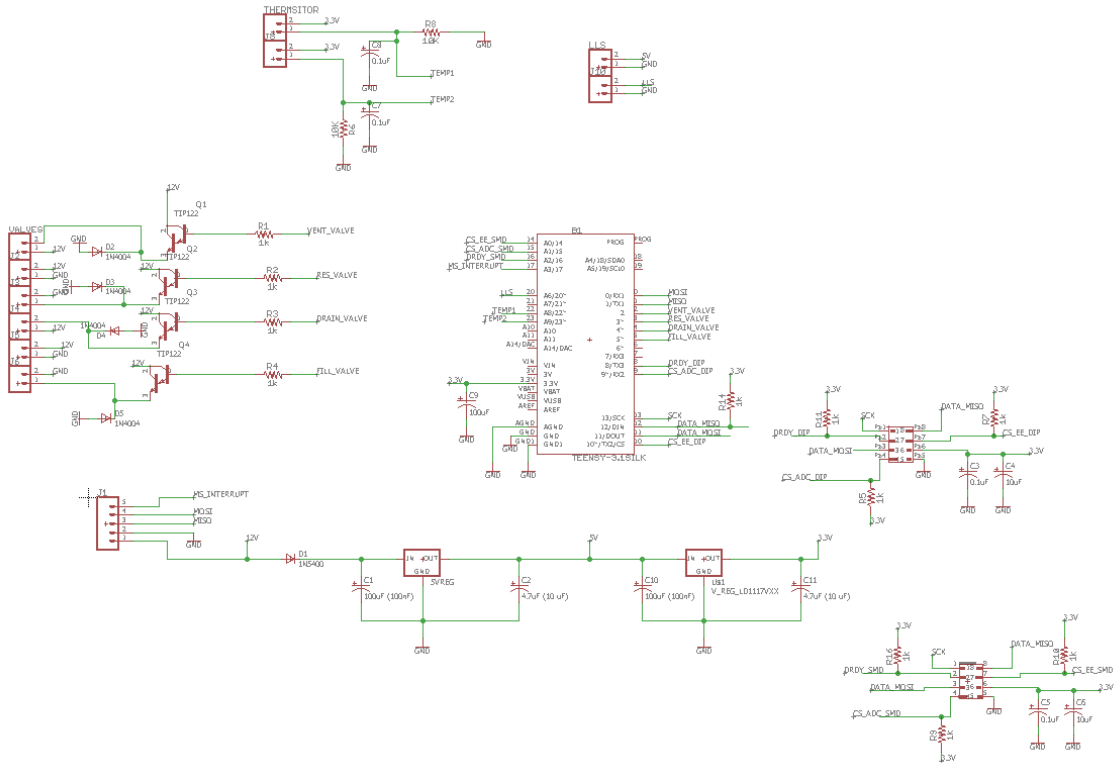

Figure A.5. The above image represents the schematic for the secondary printed circuit board.

Appendix H: Secondary Printed Circuit Board Layout

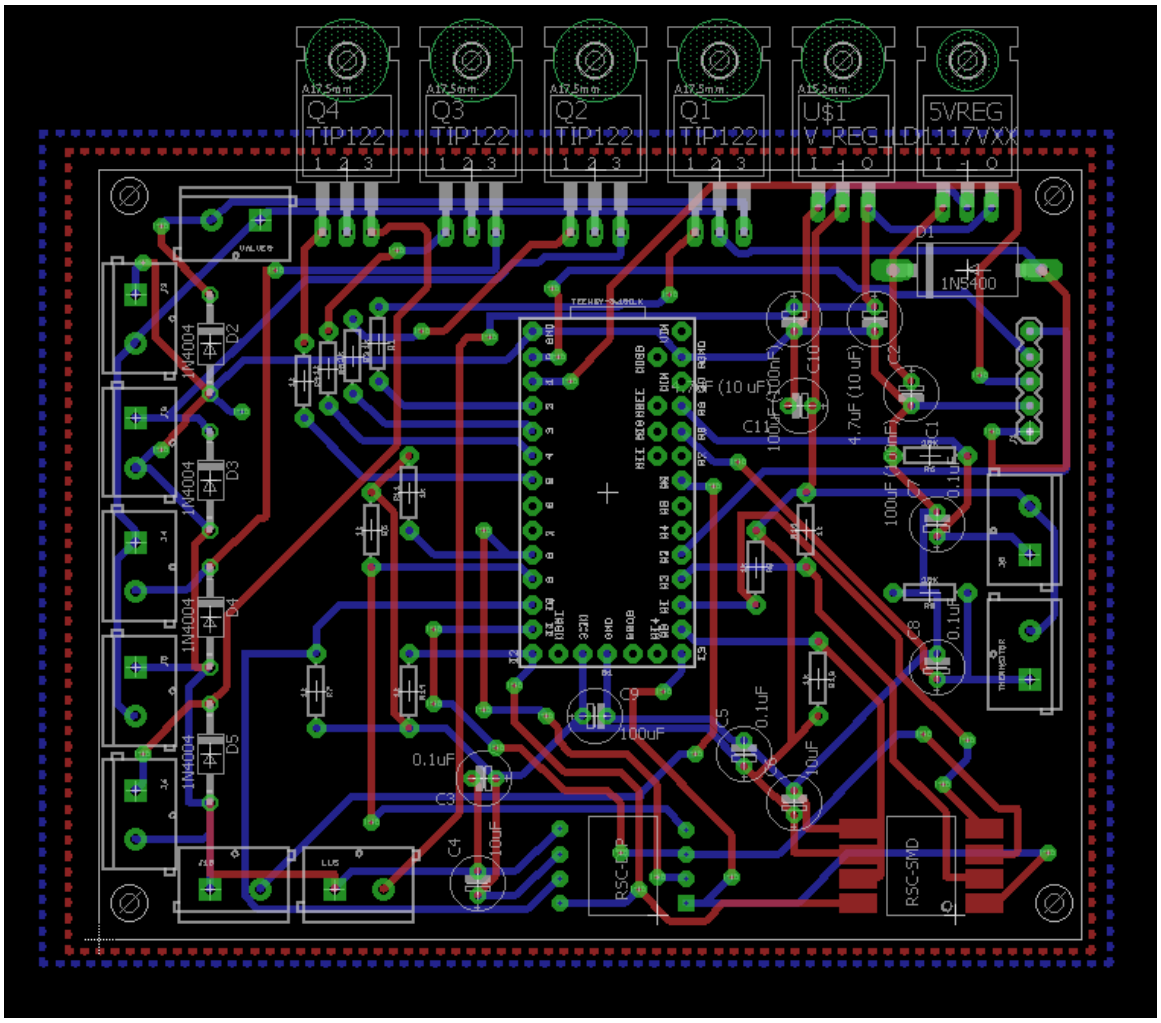

Figure A.6. The above image represents the layout for the secondary printed circuit board.

Appendix I: Initial Zero-Pressure Testing

Initial zero-pressure testing captured differential pressure readings at each temperature for the minimum and maximum pressures of approximately -1in. of water, and +2 in. of water. The -1 in. of water corresponds to the 1in. difference in height between the reference column and the sample column when both columns are full of clean water, caused by the difference in adapters used to mount the 1-inch and ½ inch ball valves on the sample and reference columns. The +2 in. of water represents the maximum positive differential pressure that the Honeywell RSC sensor can reliably capture. Testing captured raw pressure readings for these two differential pressures by first calculating the mass of water needed to raise the water level in each cylinder -1 and +2 inches respectively. Next, the METTLER PM 4000 scale precisely weighed the mass of water. After adding the measured water to the respective cylinder, the scale weighs the syringe used to inject the water to get the true mass of water added to the column. Results from these tests show that the trend of the pressure readings due to change in temperature is consistent with those conducted at a differential pressure of 0. Table A.1 shows the measured raw differential pressure with its corresponding height of water.

Table A.1. This table presents the measured raw differential pressure corresponding to the relative height of water in the PVC columns.

Raw Differential Pressure	Water Height (in)
15,726,000	-1.143
16,287,382	0.0
17,276,712	2.018

Plotting the raw pressure values taken at room temperature for the differential pressures of 0, -1 inch of water, and +2-inches of water generates a pressure compensation equation that relates the measured raw pressure differential to the calculated pressure differential in terms of inches of water added to the column. The raw pressure readings vary linearly with the corresponding changes in the height of the water, and the compensation equation is shown if Figure A.5.

It should be noted that there is variability in the establishment of the zero-pressure values. As shown in Chapter 5, the six clean water tests used to establish the zero-pressure reading varied by roughly 40,000 counts. Therefore, it is possible that the values established in this initial testing contained a similar error. If that was the case for these readings as well, the relationship established by this testing would introduce at least that much error into the measured pressure values. Once the zero-pressure reading issue is resolved, these values should be measured again and a new relationship developed.

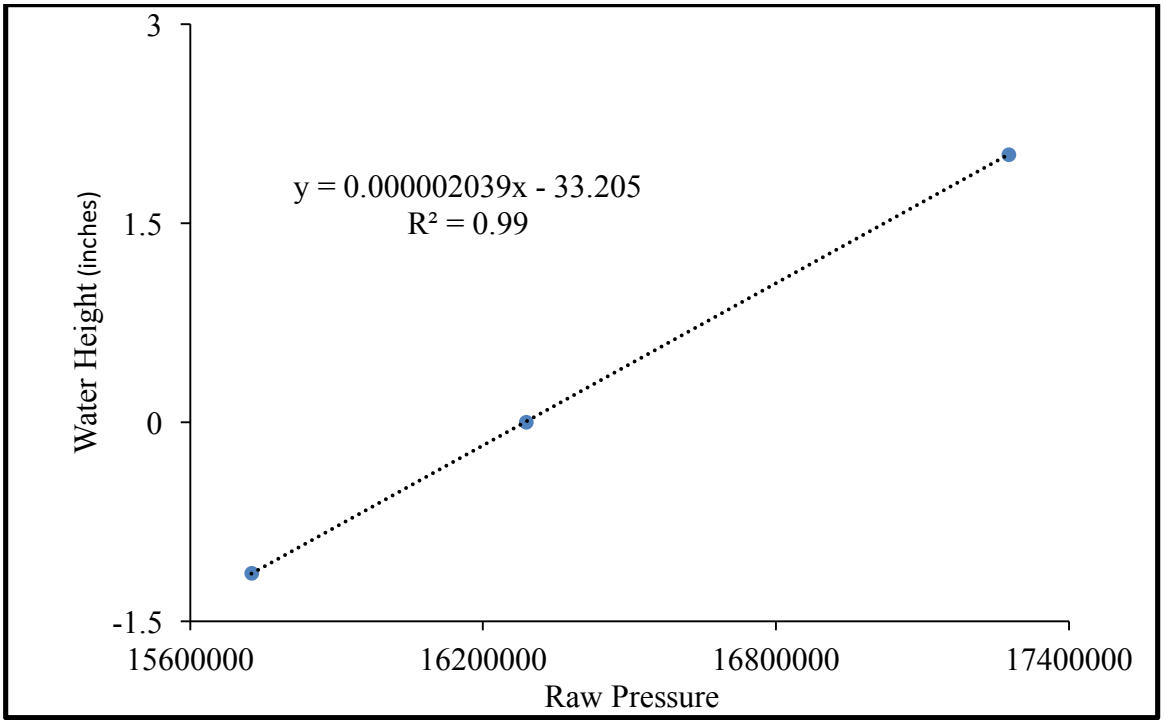

Figure A.7. This plot shows measured water height in inches on the x-axis versus the measured raw differential pressure values on the y-axis for the initial zero-pressure testing. The plot label shows the linear fit equation and R^2 value for the plotted test data.

Appendix J: Stokes Law

Stokes Law allows determination of the fall velocity (or settling velocity) of a particle in a fluid. The equation is:

$$v = \frac{2}{9}\frac{(\rho_P - \rho_F)}{u} g r^2$$

where v is the velocity in (m s^{-1}), ρ_P is the density of the particle (kg m^{-3}), ρ_F is the density of the fluid (kg m^{-3}), u is the dynamic viscosity (kg m^{-1} s^{-1}), g is the gravitational constant (m s^{-2}), and r is the radius of the particle (m).

As is evident here, a decrease in the dynamic viscosity will increase the particles fall velocity. Therefore, an increase in temperature would cause the sediment in the sample column to have a greater fall velocity.

Appendix K: Second-Generation Design Ideas

Alternative Ideas to Motorized Ball Valves:

- Motorized butterfly valves fit the current design. Mounting the valves to the PVC would require a collar. However, removing the threaded adapters currently used would decrease the places sediment can get caught inside the sample cylinder. Motors can be sized to open the valves as fast as needed, reducing the effect of the valve meniscus formation. However, sediment sticking to the valve seat may cause issues with sealing.
- Flapper valves would require additional modifications to the design. This valve probably minimizes the likelihood of leaking due to forming almost no surfaces on which sediment can accumulate. Motor can be sized to open the valves as fast as needed, reducing the effect of the meniscus formation. Might need an alternative to the liquid-level sensor as attaching PVC above the Fill valve is difficult when using a flapper valve. Suction created as the upper valve is opened may draw water out of the sample cylinder.
- Plunger or stopper valves would also provide an effective way to capture the sample volume. However, the current design would require several modifications to accommodate this valve. Alignment of the flipper arm with a motor to remove the plunger may be difficult. Motor can be sized to open the valves as fast as needed, reducing the effect of the meniscus. As with the flapper valve, sealing should not be an issue, but water being sucked out of the cylinder during opening may occur. It may be more difficult to design in such a way as to capture a very repeatable volume, since that would require inserting the stopper to exactly the same depth each time.
- NOTE: any change in valve design would require retesting to ensure that the measured volume is in fact repeatable.

Ideas for Mitigating Barb Meniscus Issues:

- Replace ¼-inch C-Flex tubing with tubing that has a water contact angle closer to 90°, reducing the force created by the meniscus. Note, however, that the contact angle between a solid and liquid is affected by surface contamination.
- Change the orientation of the ¼-inch port such that it has a 90° bend. This would force the meniscus to form in a vertical tube at perhaps a more repeatable location. However, rotation of the cylinder unit may introduce air bubbles into the port.
- Attach a screen/cover over the ¼-inch port where it threads into the sample column PVC. The screen needs to allow water to move into and out of the port while preventing sediment particles, primarily silt and clay, from depositing in the port.
- Add a small vibrator (like from a cell phone) to vibrate the meniscus of both the sample and dummy, such that the menisci achieve their equilibrium shape/pressure.

VITA

Hayden Jordan was born in Clarksville, TN, to Jeff and Patti Jordan. He is the brother of Jacob, Dylan, Salera, and Satchel. He attended Clarksville High School before enrolling at the University of Tennessee, Knoxville. In May 2016 Hayden received a Bachelor of Science degree in Biosystems Engineering at the University of Tennessee. The following fall, Hayden began his pursuit of a Master of Science degree in Biosystems Engineering from the University of Tennessee.